Cell Reports
Methods

Article

MPA$_{PASS}$ software enables stitched multiplex, multidimensional EV repertoire analysis and a standard framework for reporting bead-based assays

Graphical abstract

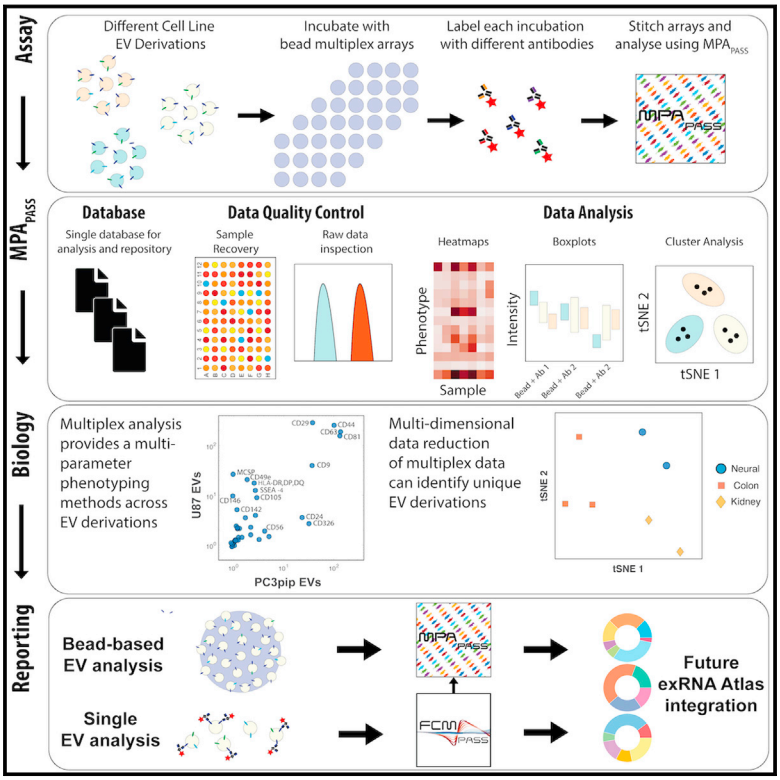

Highlights

- High-parameter EV multiplex analysis is introduced
- MPA$_{PASS}$ enables multiplex data stitching and multidimensional data visualization
- EV multiplex experiment design, performance, analysis, and reporting are presented

Authors

Joshua A. Welsh, Bryce Killingsworth, Julia Kepley, ..., Ionita Ghiran, Steve Jacobson, Jennifer C. Jones

Correspondence

jennifer.jones2@nih.gov

In brief

Welsh et al. demonstrate the utility of EV multiplex analysis with MPA$_{PASS}$ software for EV repertoire studies. MPA$_{PASS}$ enables the standard reporting and ergonomic stitching of multiplex datasets for extracellular vesicle repertoire identification.

Welsh et al., 2022, Cell Reports Methods 2, 100136
January 24, 2022
https://doi.org/10.1016/j.crmeth.2021.100136

CellPress

Cell Reports Methods

CellPress
OPEN ACCESS

Article

MPA$_{PASS}$ software enables stitched multiplex, multidimensional EV repertoire analysis and a standard framework for reporting bead-based assays

Joshua A. Welsh,[1,4] Bryce Killingsworth,[1,4] Julia Kepley,[1] Tim Traynor,[1] Sean Cook,[1] Jason Savage,[1] Jenn Marte,[2] Min-Jung Lee,[3] Hoyoung M. Maeng,[4] Michelle L. Pleet,[5] Setty Magana,[5] André Gorgens,[6,7] Cecile L. Maire,[8] Katrin Lamszus,[8] Franz L. Ricklefs,[8] Maria J. Merino,[9] W. Marston Linehan,[10] Tim Greten,[11] Tomer Cooks,[12,13] Curtis C. Harris,[13] Andrea Apolo,[14] Asim Abdel-Mageed,[15] Alexander R. Ivanov,[16] Jane B. Trepel,[3] Matthew Roth,[17] Mercedes Tkach,[18] Aleksandar Milosavljevic,[17] Clotilde Théry,[18] Amy LeBlanc,[19] Jay A. Berzofsky,[4] Eytan Ruppin,[20] Kenneth Aldape,[9] Kevin Camphausen,[21] James L. Gulley,[2] Ionita Ghiran,[22] Steve Jacobson,[5] and Jennifer C. Jones[1,4,23,*]

[1]Translational Nanobiology Section, Laboratory of Pathology, Center for Cancer Research, National Cancer Institute, National Institutes of Health, Bethesda, MD, USA
[2]Clinical Immunotherapy Section, Genitourinary Malignancies Branch, Center for Cancer Research, National Cancer Institute, National Institutes of Health, Bethesda, MD, USA
[3]Developmental Therapeutics Branch, Center for Cancer Research, National Cancer Institute, Bethesda, MD, USA
[4]Vaccine Branch, Center for Cancer Research, National Cancer Institute, Bethesda, MD, USA
[5]Viral Immunology Section, Neuroimmunology Branch, NINDS/NIH, Bethesda, MD, USA
[6]Clinical Research Center, Department for Laboratory Medicine, Karolinska Institutet, Stockholm, Sweden
[7]Evox Therapeutics Ltd, Oxford, UK
[8]Department of Neurosurgery, University Medical Center Hamburg-Eppendorf, Martinistraße 52, 20246 Hamburg, Germany
[9]Laboratory of Pathology, Center for Cancer Research, National Cancer Institute, National Institutes of Health, Bethesda, MD, USA
[10]Urologic Oncology Branch, Center for Cancer Research, National Cancer Institute, National Institutes of Health, Bethesda, MD, USA
[11]Gastrointestinal Malignancy Section, Thoracic and Gastrointestinal Oncology Branch, Center for Cancer Research, National Cancer Institute, National Institutes of Health, Bethesda, MD, USA
[12]The Shraga Segal Department of Microbiology, Immunology, and Genetics, Ben-Gurion University of the Negev, 84105 Beer-Sheva, Israel
[13]Laboratory of Human Carcinogenesis, NCI-CCR, National Institutes of Health, Bethesda, MD 20892-4258, USA
[14]Bladder Cancer Section, Genitourinary Malignancies Branch, Center for Cancer Research, National Cancer Institutes of Health, Bethesda, MD, USA
[15]Department of Urology, Tulane University School of Medicine, 1430 Tulane Avenue, New Orleans, LA, USA
[16]Barnett Institute and Department of Chemistry and Chemical Biology, Northeastern University, 360 Huntington Avenue, Boston, MA 02115, USA
[17]Department of Molecular and Human Genetics, Baylor College of Medicine, Houston, TX, USA
[18]Institut Curie, PSL Research University, INSERM U932, Paris, France
[19]Comparative Oncology Program, Center for Cancer Research, National Cancer Institute, National Institutes of Health, Bethesda, MD, USA
[20]Cancer Data Science Lab, National Cancer Institute, Bethesda, MD, USA
[21]Radiation Oncology Branch, Center for Cancer Research, National Cancer Institute, Bethesda, MD, USA
[22]Department of Medicine, Beth Israel Deaconess Medical Center, Harvard Medical School, Boston, MA, USA
[23]Lead contact
*Correspondence: jennifer.jones2@nih.gov
https://doi.org/10.1016/j.crmeth.2021.100136

MOTIVATION Assessment of EV repertoire profiles is a priority for many research groups, but methods for performing and analyzing EV markers with multimarker multiplex bead sets are not well established. MPA-PASS enables stitched multiplex EV analyses, and our results illustrate key considerations for designing, performing, and analyzing EV multiplex studies.

SUMMARY

Extracellular vesicles (EVs) of various types are released or shed from all cells. EVs carry proteins and contain additional protein and nucleic acid cargo that relates to their biogenesis and cell of origin. EV cargo in liquid biopsies is of widespread interest owing to its ability to provide a retrospective snapshot of cell state at the time of EV release. For the purposes of EV cargo analysis and repertoire profiling, multiplex assays are an essential tool in multiparametric analyte studies but are still being developed for high-parameter EV protein

detection. Although bead-based EV multiplex analyses offer EV profiling capabilities with conventional flow cytometers, the utilization of EV multiplex assays has been limited by the lack of software analysis tools for such assays. To facilitate robust EV repertoire studies, we developed multiplex analysis post-acquisition analysis (MPA_{PASS}) open-source software for stitched multiplex analysis, EV database-compatible reporting, and visualization of EV repertoires.

INTRODUCTION

Extracellular vesicles (EVs) are submicron phospholipid bilayer-enclosed spheres secreted from cells. EVs carry proteins on their surface as well as intracellular cargo in the form of proteins, nucleic acids, metabolites, lipids, and others. EV research is a rapidly developing area due to its prospective use as translational biomarkers and therapeutics (Matsuzaki and Ochiya, 2017; Reiner et al., 2017). However, the utilization of EVs is hampered by currently available analysis methods.

The majority of EVs have been demonstrated to be $\leq$100 nm in diameter, with a power-law distribution ranging from $\sim$25 to >1,000 nm (van der Pol et al., 2014; Tian et al., 2020; Lennon et al., 2019). A wide variety of detection methods have been utilized for characterizing single EVs (Issadore et al., 2011; Shao et al., 2010, 2012; Lennon et al., 2019; Tian et al., 2018; van der Pol et al., 2010, 2013, 2018). A current limitation of EV characterization in the field is the sensitivity of single-EV phenotyping assays. The low numbers of expressed proteins on the surface of EVs make the use of common high-throughput, single-particle phenotyping techniques such as flow cytometry and confocal microscopy particularly difficult due to having sensitivities ranging from >10 to 1,000 molecules of a given fluorophore (Gasecka et al., 2020; Tertel et al., 2020; Welsh et al., 2020b). More recently, a commercially available, dedicated, small-particle flow cytometer has shown the ability to enumerate the majority of EVs and demonstrate fluorescence sensitivity for <10 molecules of phycoerythrin (Zhu et al., 2014; Tian et al., 2020). This has important implications for accurately enumerating EV phenotypes and counts within clinical samples. It is only with single-molecule detection that we can confidently state that EVs may be negative for a given marker at a single particle level (Tian et al., 2018). However, this technique is limited to one color in this single-molecule sensitivity range and therefore requires prior knowledge of subset markers to identify within a sample.

A method that has been used by the EV field to semi-quantitatively enable EV phenotyping of dim markers is to use a multiplex array of fluorescently bar-coded antibody capture beads in combination with a detection antibody (Koliha et al., 2016; Wiklander et al., 2018). This allows potentially hundreds to thousands of EVs with a commonly expressed protein to attach to the surface of a single 5–8 μm bead conjugated with an antibody for that protein. A fluorescently conjugated detection antibody is then used to confirm EV-binding to any specific bead. While useful, single bead-based assays offer limited utility to understand the heterogeneous phenotypes of EVs compared with multiplex arrays. A particular advantage of bead-based assays is their ability to be run on conventional cytometers. While newer-generation cytometers with more sensitivity and a larger dynamic range are beneficial, in many cases legacy instruments can be sufficient for phenotyping EVs.

More recently, EV multiplex kits have become available, enabling the simultaneous use of up to 39 distinct antibody-capture beads (Koliha et al., 2016; Wiklander et al., 2018). While this commercially available kit is sold with three detection antibodies for tetraspanins (CD9, CD63, and CD81), the kit is compatible with any detection antibody provided it fluoresces in a region of the spectrum not occupied by the fluorophore-coated beads. However, the utilization of this method of analysis quickly generates large quantities of data. With each tetraspanin detection antibody being used separately, 111 protein combinations are generated with six bead controls per sample. Analysis of this scale of data is currently limited by a lack of software analysis tools.

Here, the use of stitched multiplex analysis, which provides a method to survey the expression of hundreds of protein combinations on EVs, is evaluated. Considerations for undertaking multiplex analysis for surveying EV repertoires are also outlined. The ability to perform stitched multiplex analysis to analyze data on this scale is demonstrated using a lab-built, open-source software package (multiplex analysis post-acquisition analysis software [MPA_{PASS}]) that allowed for high-throughput, multiparametric quality control and data analysis of EV multiplex data. In this work, we use a commercially available EV multiplex kit, and this pipeline is compatible with any combination of bead-based assays.

RESULTS

Interpreting EV multiplex outputs

Unlike a typical multiplex assay or an ELISA in which there is a single analyte measured per capture antibody, EV multiplex assays capture a heterogeneous set of particles with respect to size and composition. These captured particles then have their other surface analytes probed with detection antibodies (Figures 1A–1D). This, therefore, leads to differences in interpretation and analysis compared with traditional multiplex analysis. Because EVs express multiple different proteins on their surface, the signal obtained from each bead is dependent both on the relative expression and heterogeneity of EVs and on the other capture beads that are present in the multiplex set (Figure 1A). The signal intensity as well as the variation can therefore encode useful information about the epitope abundance and population heterogeneity (Figures 1E and 1F). Optimal data scaling will also differ from typical multiplex and ELISA assays, as the binding capacity of the analyte to the capture antibody is fixed, allowing calibration into standard units, such as μg. Unlike these assays, the binding capacity of the detection analyte depends on the number of captured EVs on a bead, their diameter, and their expression. These could, therefore, differ drastically between each capture bead. How signals are normalized and interpreted will greatly affect reported results, as shown in Figures 1G and

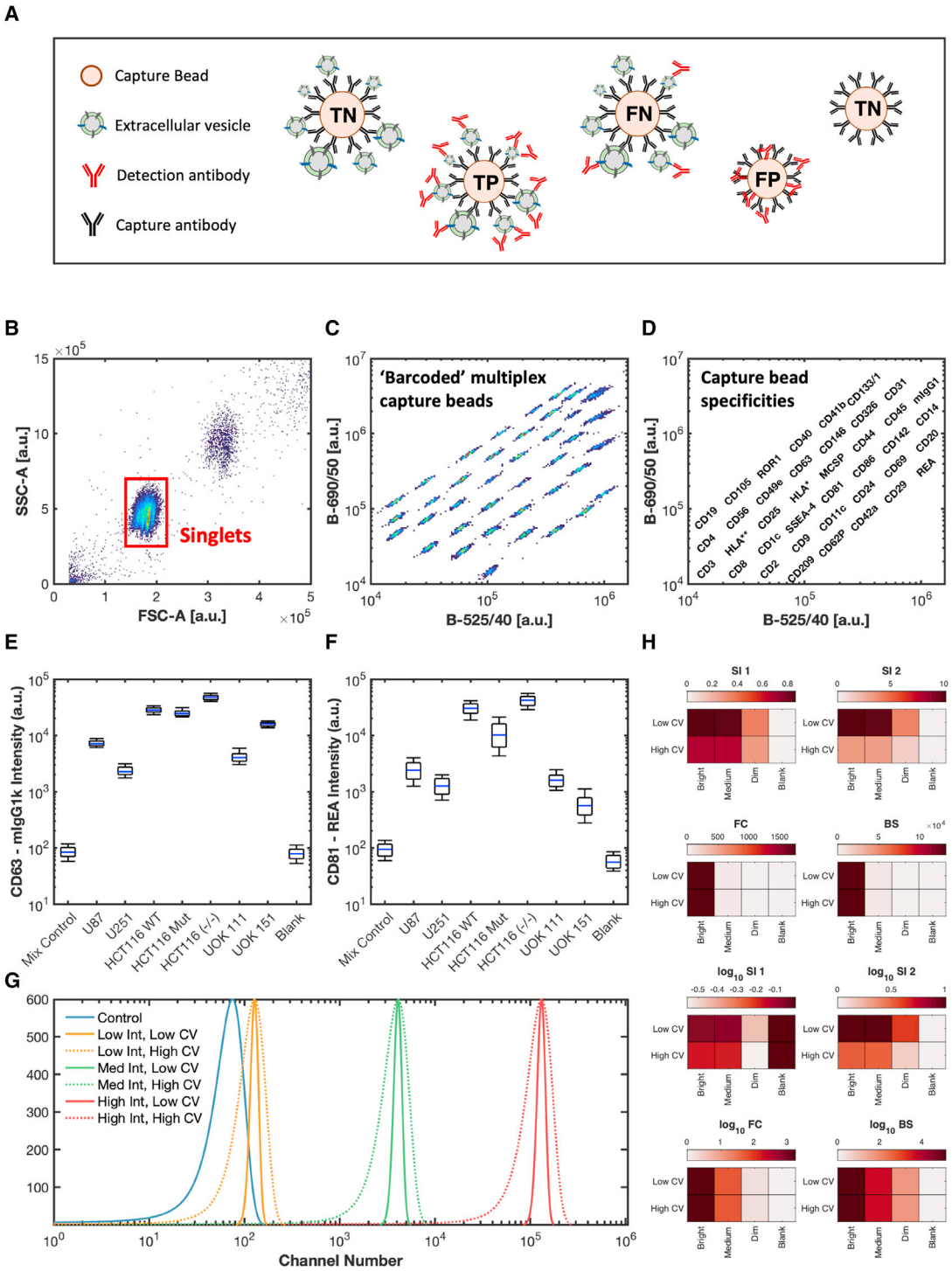

Figure 1. EV multiplex array overview and signal interpretation

(A) Illustration of different scenarios leading to obtained signal from each capture bead. Capture beads are: TP, true positive; FP, false positive; FN, false negative; and TN, true negative.

(B) Gating of singlet bead populations on forward (FSC-A) and side (SSC-A) signals.

(C) Capture bead population fluorescent "bar coding" in the multiplex array using 488 nm illuminations and collection at 525/40 and 690/50.

(D) Specificity of each capture bead population shown in (C).

(legend continued on next page)

1H. It is clear from these data that a multiplex analysis using EVs and not soluble proteins, for which many are generally intended, is limited when the data are interpreted in linear units. Using a logarithmic scale regardless of the normalization algorithm allows for the differentiation of high, medium, and dim signals from a control population. While there is no clear solution to differentiate high from low coefficients of variation (CVs) with any of the algorithms when using linear scaling, using a form of separation index is more capable of differentiating dim signals from a control population compared with fold-change or background subtraction. While background subtraction may be commonly used with different assays, due to the reliance on logarithmic scaling, it poses challenges resulting from the creation of negative numbers that cannot be scaled logarithmically. While SI1 and SI2 are commonly used in the flow cytometry field, their use in interpreting multiplex data may lead to ambiguous data given the influence of CVs in differentiating the positivity of a signal. For our work, we chose to use log-scaled metrics in the form of fold-change and background subtraction that were unaffected by CVs to differentiate signals.

Signal interpretation of EV multiplex assays is not dissimilar from traditional multiplex assays and ELISAs with true positives, true negatives, false positives, and false negatives possible (Figure 1A). Like single-EV flow cytometry, false negatives may be prevalent either because not enough EVs bind to bead populations to provide a sufficient signal or the number of expressed proteins is too low to provide a sufficient signal to be detected.

EV multiplex controls: Sample titration

As with all assays, controls are important to ensure the reliability of data. Typically, assays quantifying proteins based on fluorescence intensity will use standards to create a titration curve to convert fluorescence intensity to a concentration measurement. Due to EVs differing in surface area and epitope abundance and expressing multiple proteins that will affect binding affinity to multiplex capture beads, the use of titration to quantitate the EV number is not a robust measure using EV multiplex assays. Whereas using titration for a quantitative EV measurement output is unreliable, the inclusion of titration controls is critical given the nonspecificity that can arise with detection antibodies binding to beads. A titration of PC3pip and U87 EV input material from 10^6 to 10^{10} with ~20,000 total beads (Figures 2A and 2B; Figure S2) demonstrates the effect of titration on the signal intensity of a CD9, CD63, and CD81 detection antibody cocktail. Capture beads CD81, CD63, CD44, and CD29 show an expected increase in signal intensity with increasing EV input material across both PC3pip and U87 EVs. Most markers show little nonspecific binding with the CD9, CD63, and CD81 detection antibody cocktail; however, there does appear to be a consistently increased background signal compared with blank beads from markers SSEA-4, CD105, CD56, and CD25 irrespective of the input material (Figure S2). The appearance of staining distinguishable from the background begins at 10^8 and 10^9 total EVs for U87 and PC3pip, respectively. However, this amount of input material is relative to the ~20,000 total beads incubated. The increase in signal intensity with input EV counts from 10^9 to 10^{10} differs depending on the capture bead and EV source, highlighting the multifactorial binding kinetics and semiquantitative nature of this assay. This is further highlighted by looking at the relationships among markers across EV cell-line derivation (Figures 2A and 2B). While the relationship of epitope abundance from 10^9 to 10^{10} is preserved, the change in intensity across markers would not necessarily be predictable without first having done a titration of input material. Given a high enough amount of input material, such as 10^{10} EVs, the intensity of the CD9, CD63, and CD81 detection antibody cocktail across numerous beads provides a high enough signal intensity to be able to make distinctions among expressed marker intensity EV cell lines (Figures 2A and 2B). CD81, CD63, CD44, and CD29 are highly expressed across both U87 and PC3pip EVs, whereas CD24 and CD326 show a higher abundance in PC3pip EVs and MCSP (CSPG4, NG2), CD49e, and human leukocyte antigen (HLA)-DR, -DP, and -DQ, showing a higher abundance in U87 EVs. We recommend the use of a sample titration for multiplex sample input either in a concentration- or volume-dependent manner, depending on the assay, as a method to show the antibody detection signal is titrating with the sample input.

EV multiplex controls: Identifying nonspecific signals

Identifying the nonspecific binding of detection antibodies to capture beads is critical for the reproducibility and interpretation of data. A capture bead with a detection antibody alone as a control is critical in all assays. One test investigated the efficacy of 17 alternative detection antibodies (Table 1) to CD9, CD63, and CD81 using two different blocking buffers across the 39-capture bead array. U87 and U251 cell-line-derived EVs were also included as positive controls. A selection of the capture bead markers is shown in Figure 3 (full array in Figure S3). This screening of custom antibodies with the commercial bead-based assay demonstrates that nonspecific binding of the antibody can be capture-bead-dependent. For example, CD147 detection of CD44 capture beads demonstrates a high signal on U87 EVs and, to a lesser extent, U251 EVs. The bead + antibody control in this example shows minimal binding. Capture beads such as CD1c show an undetectable signal for CD147, whereas the CD31, CD133/1, and CD326 capture beads show a dim positive signal for the CD147 detection antibody and have a lower signal for the bead + sample + antibody. This indicates a small amount of nonspecific binding. This may be reduced by EVs due to the EVs blocking antibody binding to the beads before antibody incubation. In this comparison, we also included 2% EV-depleted FBS as a control. The EV-depletion method using ultracentrifugation shows that a number of

(E and F) Data of (E) CD63 and (F) CD81 capture beads with detection of 1 × 10^9 EVs from different cell derivations using CD9, CD63, and CD81 detection antibody mixture.

(G) Artificial flow cytometry signals of a control bead, along with a high-, medium-, and low-intensity bead with high and low variance.

(H) Interpretation of data from (C) using different normalization methods with linear and logarithmic scaling. Normalization formulas (separation indexes 1 and 2 [SI1,2], fold change [FC], and background subtraction [BS]) are outlined in the methods.

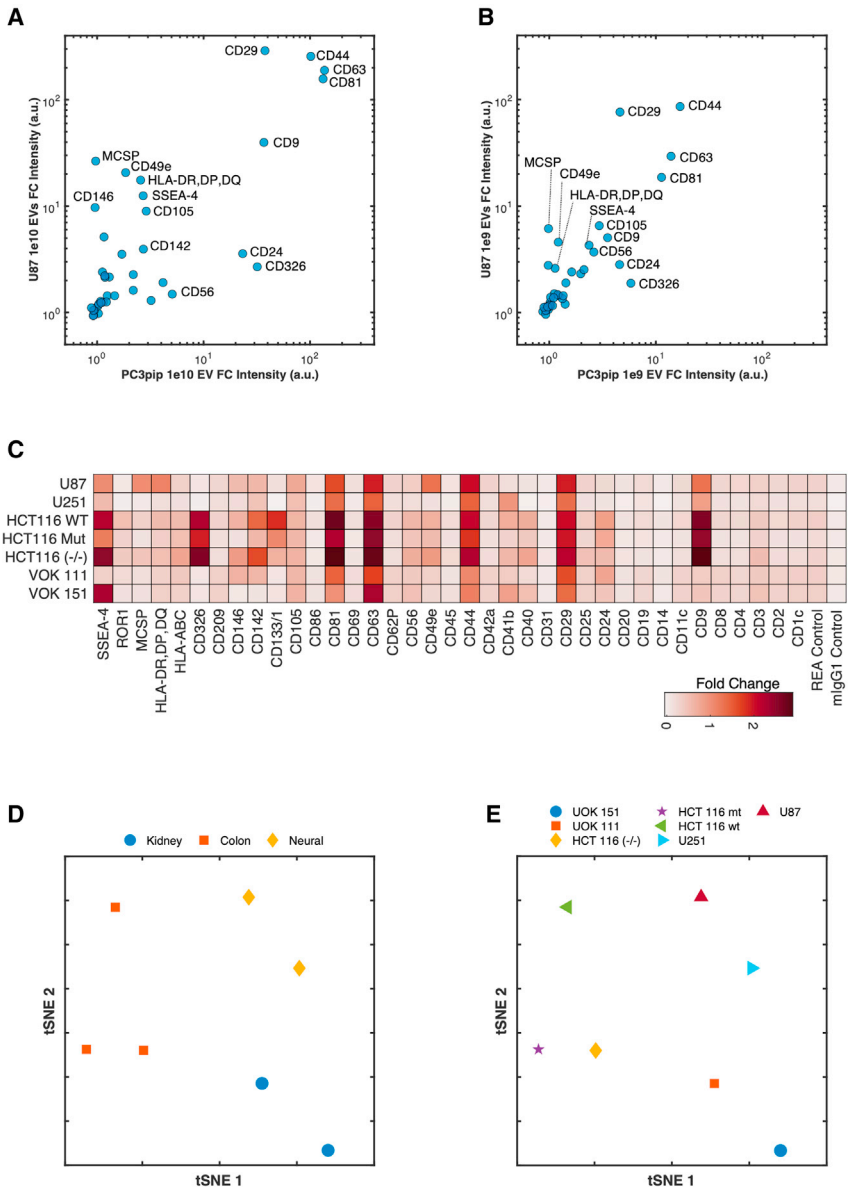

Figure 2. Effect of input material on signal and identifying unique marker combinations between EV derivations

(A and B) Scatterplot of bead intensities incubated with 1×10^{10} and 1×10^{9} EVs from U87 and PC3pip cell lines.

(C) Heatmap of detection intensities of EVs from kidney (VOK111 and VOK151), colon (HCT116wt and mt, −/−), and neural (U87 and U251) cell derivations.

(D and E) Beads were incubated with 1×10^{9} EVs and detected using an EV mix (CD9, CD63, and CD81). tSNE was performed on samples, stratifying them by tissue derivation (D) and cell line (E).

EV multiplex analysis identifies cell-line tissue derivation

Multiplex analysis of EVs derived from neural, kidney, and colon cell lines using just a cocktail of CD9, CD63, and CD81 tetraspanins as detection antibodies was performed to identify whether EVs from different tissues had unique expression profiles (Figures 2C–2E). HCT116 cell lines show a higher intensity compared with kidney and neural cell lines with markers including CD326, CD133/1, CD81, and ROR1 being exclusively expressed and undetectable on neural and kidney EVs (Figure 2C). The variations in expression can be visualized among cell lines from the same tissue from heat map visualizations (Figure 2C).

Although all other capture beads, such as CD9, stain positively for the tetraspanin detection antibody mix, the expression levels vary considerably among EV tissue derivations. For example, EVs from the colon cell line expressing high levels captured on the CD9 bead stain brightly for the tetraspanin mix, whereas the kidney EVs stain very dimly, and the neural EVs stain at an intermediate level (Figure 2C). These differences further highlight the heterogeneity of EVs and demonstrate that CD9, CD63, and CD81 may not be present on all EVs.

positive signals can have a better result compared with Miltenyi Biotec buffer alone. It is notable that the etraspanin signals CD9, CD63, and CD81 are all lower when samples are incubated in EV-depleted FBS, and this indicates that small EVs remain after the depletion method and may be able to compete with cell-culture-derived EVs to varying degrees with cross-reactive antibodies for both capture and detection. It is notable that one antibody, CD47, bound to every capture bead regardless of buffer. These data demonstrate the need to screen detection antibodies with capture beads before use. This is also plotted by ordering the average intensity across groups with the top 75 summarized in Figure S4. For this reason, while including bead + antibody controls is essential, subtracting the bead + antibody intensity for bead + EVs +antibody is not recommended, asit may result in negative intensity data scaling.

Use of clustering to identify difference between biofluid and purification

The use of multiplex analysis in sample cohorts can result in large arrays of data. Our proposed method of stitched multiplex analysis further increases that size. Methods of data reduction to identify populations in large datasets are beginning to become commonplace (e.g., t-distributed stochastic neighbor embedding [tSNE]). With the accumulation of data across samples, equipment, assays, laboratories, and data reduction methods will play a role in understanding differences and similarities. For this reason, principal-component analysis (PCA) and tSNE

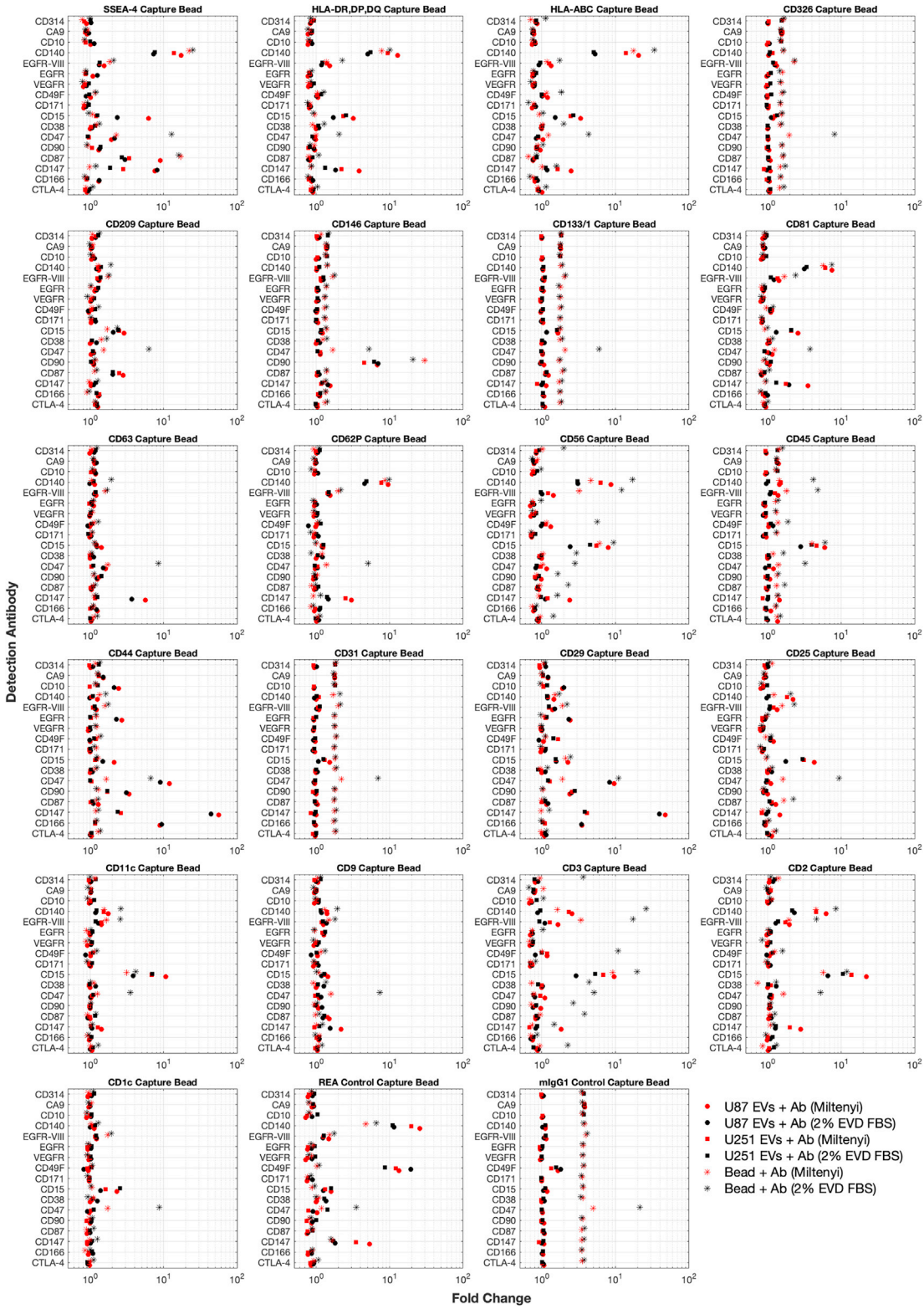

Figure 3. Screening antibodies for nonspecific binding

A selection of capture beads when incubated with 0.5 μg of detection antibody with buffer (asterisks) was incubated as negative controls. EV samples derived from U87 (circles) and U251 (squares) cell lines were used as positive controls. The included Miltenyi buffer (shown in red) and 2% EV-depleted FBS (shown in black) were also compared.

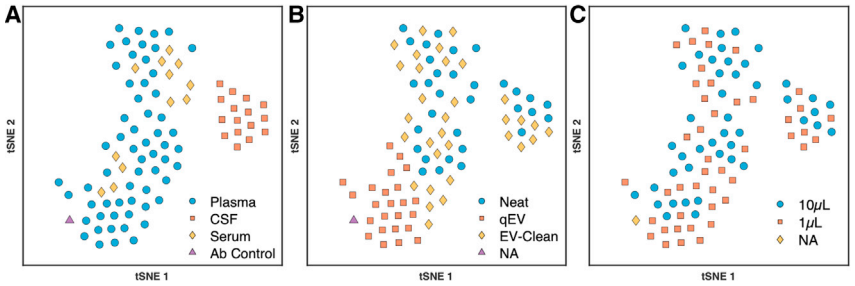

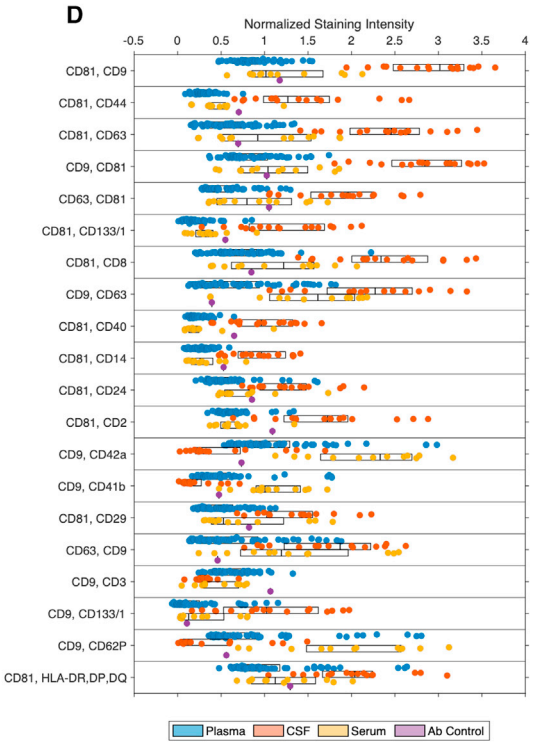

Figure 4. Clustering of samples from differing biological fluids

(A–D) tSNE was performed on data from samples of plasma, serum, and CSF and stained with CD9, CD63, and CD81 across 39 unique capture beads and stratified by biological fluid (A), isolation method (B), and volume (C). (D) Boxplot of the top 25 capture bead and detection antibody combinations across samples showing the most significance as determined by Kruskal-Wallis.

have been built into MPA_{PASS}. To understand the utility data reduction methods bring to stitched multiplex analysis plasma, serum, and CSF samples were analyzed using tetraspanins CD9, CD63, and CD81 individually at different input volumes and with different sample purification methods (Figure 4). Figure S5 shows the resulting heatmap of this large dataset when hierarchically clustered. At a high level,it can be seen that there appear to be areas of capture-detection marker enrichment between the plasma and CSF sample sources.

An alternative method of visualizing similarities and differences across this dataset with a means to stratify by metadata, such as by purification or input material volume, is tSNE analysis. Using tSNE analysis, it is possible to separate CSF from plasma and serum (Figure 4A). This separation was independent of the sample purification method or input volume (Figures 4B and 4C). Serum and plasma samples prepared with qEV columns, however, cluster separately from neat and EV-clean samples. By looking at the top 25 most significant group differences (Figure 4D) it can be seen that the predominant differences are increased intensities of classical EV tetraspanin detection: CD9, CD63, and CD81, but also immune and stemness marker detection: CD8, CD14, CD24, CD40, and CD44. Serum and plasma groups both showed increased detection for platelet markers CD41b, CD42a, and CD62P. Preliminary data suggest that multiplex arrays can differentiate between samples from platelet-rich plasma (PRP) and platelet-poor plasma (PPP) and in different isolation tubes (Figure S6). These data demonstrate the utility of data reduction methods potentially for sample identification as well as batch effects such as different isolation methods among sample cohorts that may occur in aggregation methods such as the creation of an atlas.

Many plasma samples in clinical protocols are frozen while still containing platelets, which is not recommended within the EV field. The phenotypic difference of platelet depletion was investigated before samples were frozen and a comparison of fixed versus non-fixed blood isolation tubes was shown using the ratio of PPP to PRP for Streck and EDTA isolation tubes from a matched sample time point (Figure S6). It was seen in this isolated case that PPP contained a higher detection intensity for tetraspanins CD63 and CD81, platelet markers CD41b, CD42a, and CD62P, and immune markers CD8 and CD69 than did PRP. These results indicate that the thawing process and the subsequent platelet depletion protocol may remove more platelet EVs than when the platelet depletion protocol is conducted prior to freezing.

Fewer differences can be seen between the ratio of PRP to PPP plasma in fixed versus non-fixed isolations tubes. CD1c, CD14, and CD20 intensities are slightly higher in EDTA versus Streck tubes, whereas CD69 and CD4 intensities appear to be slightly higher in Streck versus EDTA tubes. Whether these changes are due to the number of particles present or the effect of the fixative on the epitope itself requires further investigation.

MPA_{PASS} facilitates data sharing and atlas curation

MPA_{PASS} was developed in response to the lack of commercially available or free software packages for EV multiplex analysis. As

Table 1. Detection antibodies used

Target	Labeling	Fluorescent	Isotype	Clone	Manufacturer	Catalog
CD9	5 μL	APC	mouse IgG1	proprietary	Miltenyi Biotec	130-108-813
CD63	5 μL	APC	mouse IgG1, κ	proprietary	Miltenyi Biotec	130-108-813
CD81	5 μL	APC	REA	proprietary	Miltenyi Biotec	130-108-813
CTLA-4	0.5 μg	APC	mouse IgG2a, κ	BNI3	BioLegend	369612
CD166	0.5 μg	APC	recombinant human IgG1	REA442	Miltenyi Biotec	130-106-576
CD147	0.5 μg	APC	mouse IgG1, κ	HIM6	BioLegend	306214
CD87	0.5 μg	APC	recombinant human IgG1	REA892	Miltenyi Biotec	130-114-851
CD90	0.5 μg	APC	mouse IgG1, κ	5E10	BioLegend	328114
CD47	0.5 μg	APC	mouse IgG1, κ	CC2C6	BioLegend	323124
CD38	0.5 μg	APC	mouse IgG1, κ	HIT2	BioLegend	303510
CD15	0.5 μg	APC	mouse IgM, κ	HI98	BioLegend	301908
CD171	0.5 μg	APC	recombinant human IgG1	REA163	Miltenyi Biotec	130-100-684
CD49F	0.5 μg	APC	rat IgG2a, κ	GoH3	BioLegend	313616
VEGFR	0.5 μg	APC	mouse IgG1κ	ES8-20E6	Miltenyi Biotec	130-093-601
EGFR	0.5 μg	APC	mouse IgG1, κ	AY13	BioLegend	352906
EGFRvIII	0.5 μg	AF647	mouse IgG1, κ	DH8.3	Novus Biologicals	NBP2-50599AF647
CD140	0.5 μg	APC	mouse IgG1, κ	18A2	BioLegend	323608
CD10	0.5 μg	APC	mouse IgG1κ	97C5	Miltenyi Biotec	130-093-450
CA9	0.5 μg	APC	recombinant human IgG1	REA658	Miltenyi Biotec	130-110-058
CD314	0.5 μg	APC	mouse IgG1κ	1D11	BioLegend	320808

IgG, immunoglobulin G; VEGFR, vascular endothelial growth factor receptor; EGFRvIII, epidermal growth factor receptor variant III.

demonstrated, MPA_{PASS} provides researchers with normalization methods, multiplex data stitching capabilities, data reduction methods, and data visualization methods in open-source software.

Along with a lack of software interfaces for EV multiplex analysis, there is also a current a lack of reporting standards for bead-based assays within the EV field. MPA_{PASS} has attempted to facilitate this by being built on a standard database framework in the form of a spreadsheet containing key metadata criteria related to the assay (Table 2). This spreadsheet database framework (see key resources table) provides set sample, capture, and labeling metadata criteria for users to complete and allows users to further define their own metadata fields for stratification of their data analyses. Databases can also be merged to create aggregate datasets, making it possible to create personal atlases. While all metadata are found within a spreadsheet, once imported into the software, all data and metadata are then stored in a single file in order to simplify data sharing. Metadata related to cytometer acquisition are already developed in the form of MIFlowCyt. Software for the calibration of data and the automated reporting of acquisition metadata has already been established using previously developed FCM_{PASS} software.

DISCUSSION

Here, we have demonstrated a software pipeline and controls that enable the ergonomic analysis of hundreds to thousands of protein combinations on EVs using stitched multiplex analysis. This tool is a powerful method of identifying potential markers for downstream high-sensitivity, single-EV assays, such as high-sensitivity flow cytometry or super-resolution microscopy (Lennon et al., 2019; Tian et al., 2018). Alternatively, this method could be used to identify markers for targeted subset isolation methods that could be used for subsequent downstream bulk assays such as RNA sequencing. Stratifying RNA sequencing data by protein subsets could provide novel insights into EV derivation in complex fluids building on previously developed deconvolution algorithms (Murillo et al., 2019). The MPA_{PASS} software has been developed for the future curation of datasets into the existing ERCC exRNA Atlas in mind (Figure 5) (Murillo et al., 2019). The software is part of a package of tools developed for standardized reporting and analysis. While MPA_{PASS} provides these tools for bead-based EV analyses, its counterpart, FCM_{PASS}, provides standardized reporting and analysis tools for single-EV flow cytometry experiments, utilizing the MIFlowCyt-EV reporting framework (Welsh et al., 2020a, 2020d, 2020e; Welsh and Jones, 2020). FCM_{PASS} may also be used for '.fcs' file calibration prior to MPA_{PASS} data import for fluorescence calibration (Welsh and Jones, 2020). The use of these standardized reporting and analysis methods will aid in the transparency, reproducibility, and integration of EV repositories that will allow new approaches to EV characterization and subset identification.

One key consideration for the future of EV repertoire analysis with multiplex assays is that reproducibility and standardization across studies with these assays is an area for further development. A number of steps can be taken to improve assay quality and standardization: (1) quantification of the binding capacity of each bead in order to help standardize lots and

Table 2. Default MPA_{PASS} reporting framework criteria

Criteria	Sheet	Description
Sample_Filename_Prefix	Sample	name of raw data file
Sample_Set_ID	Sample	numeric set ID of sample if stitched analyses are being used
Sample_ID	Sample	descriptive ID of sample
Sample_Grouping_ID	sample	primary sample testing group (e.g., treated/untreated)
Sample_Control_ID	sample	control set ID being used for normalization
Sample_Control_Filename	sample	name of raw data file for the control
Sample_Label_Mix_No	sample	detection antibody cocktail mix number
Incubated_Sample_Volume	sample	volume of sample incubated
Incubated_Sample_Concentration_per_mL	sample	concentration of sample incubated
Sample_Source	sample	source of sample (e.g., cell culture, plasma)
Sample_Isolation_Tube	sample	tube used to isolate EVs (e.g., ethylenediaminetetraacetate, heparin)
Sample_Purification_Method	sample	method used to purify EVs
Sample_Incubation_Time_With_CaptureBead	sample	sample incubation time with capture bead
Sample_Incubation_Time_With_Antibody	sample	sample incubation time with detection antibody
Antibody_Wash_Method	sample	method to wash excess antibody
Flow_Cytometer	sample	cytometer on which control data were acquired
Bead_Identifier	beads	unique identify for multiplex array
Bead_CaptureAntibody_Target	beads	bead capture antibody target
Bead_CaptureAntibody_Isotype	beads	bead capture antibody isotype
Bead_Capture_Antibody_Clone	beads	bead capture antibody clone
Bead_Wash_Buffer	beads	bead wash buffer
Bead_Capture_Antibody_Manufacturer	beads	bead capture antibody manufacturer
Bead_Capture_Antibody_CatNo	beads	bead capture antibody catalog number
Bead_Capture_Antibody_LotNo	beads	bead capture antibody lot number
Bead_Diameter	beads	bead diameter
Bead_Manufacturer	beads	bead manufacturer
Bead_Conjugation_Molecule	beads	bead conjugation method
Bead_Volume_Incubated	beads	bead volume incubated
Bead_Count_Incubated	beads	bead count incubated
Mix_Number	labeling	detection antibody cocktail mix number
Import_Column_Number	labeling	column relating to the specific detection antibody data within raw data file
Label_Target	labeling	target of the detection antibody
Label_Fluorophore	labeling	fluorophore conjugated to the detection antibody
Label_Isotype	labeling	isotype of the detection antibody
Label_Manufacturer	labeling	manufacturer of the detection antibody
Label_Catalogue_Number	labeling	catalog number of the detection antibody
Control_Filename_Prefix	controls	name of the raw data file
Control_Set_ID	controls	set to which control data relate
Control_Name	controls	name of control (e.g., blank bead)
Sample_Label_Mix_No	controls	mix number to which control relates
Control_Incubation_Time_With_Antibody	controls	detection antibody incubation time with control (if applicable)
Antibody_Wash_Method	controls	method used to wash excess antibody (e.g., filter plate)
Flow_Cytometer	controls	cytometer on which control data were acquired

Outlined are reporting metadata database fields generated upon MPA_{PASS} dataset creation. Each criteria field is created within the spreadsheet and is organized onto sheets within the spreadsheet relating to sample, beads, labeling, or controls.

bead types; (2) development of custom multiplex arrays that contain pathology-specific monoclonal capture antibodies, with matched individual monoclonal capture beads for validation assays and pull down; (3) potential use of Molecules of Equivalent Soluble Fluorophore (MESF) standards for calibration and comparison of data among instruments; and (4) development

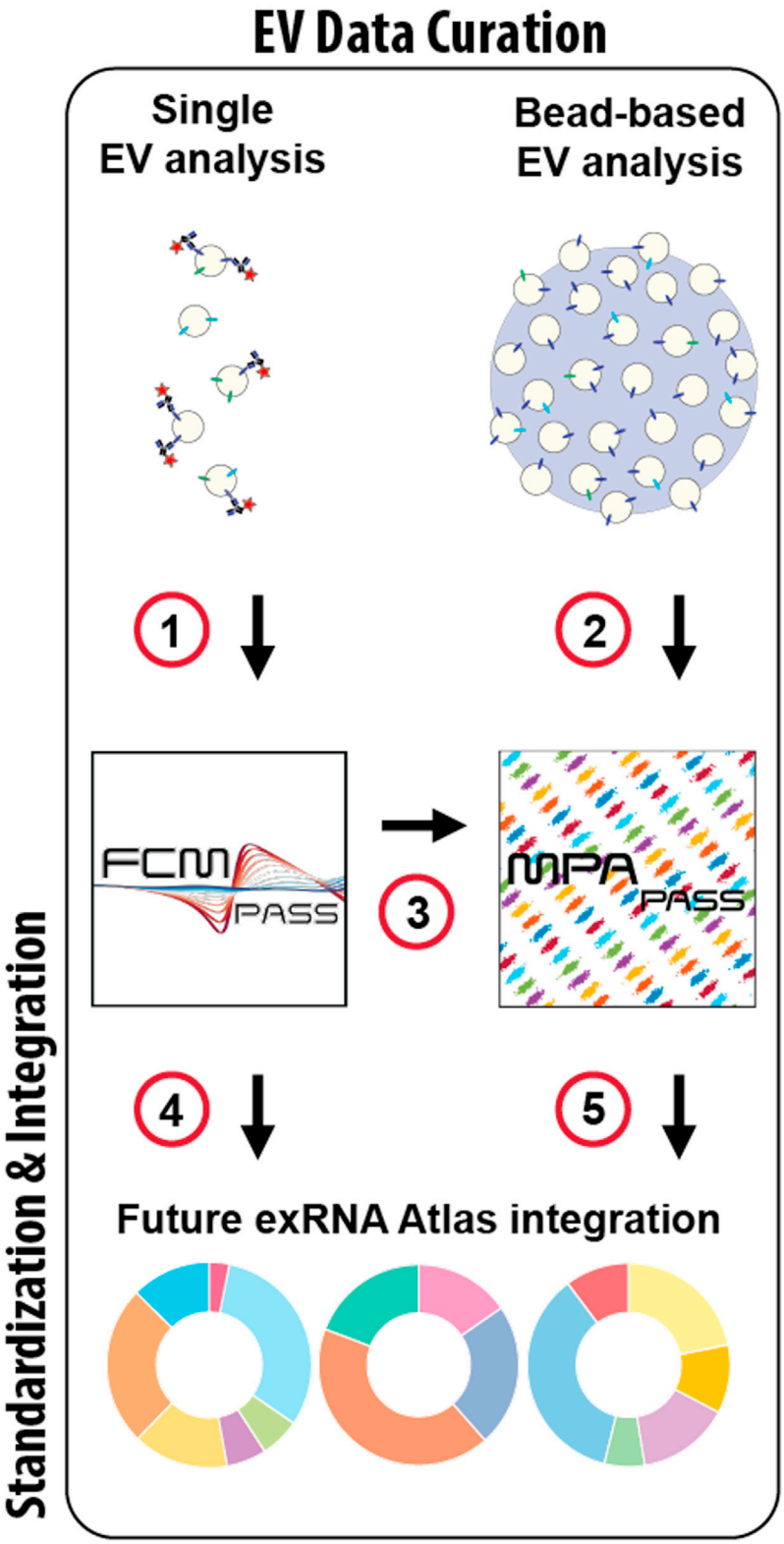

Figure 5. Pipeline for single-EV and bead-based assay EV Atlas curation

The processing of single-EV data (1) using FCM_{PASS} and bead-based assays and (2) using MPA_{PASS} software produces standard reporting methods and data. MPA_{PASS} data can be calibrated with FCM_{PASS} (3) software or other means. The product of these software packages is the integration of single-EV data (4) and bead-based EV data (5) that will enable standard comparisons and reporting for integration into online repositories such as the exRNA atlas.

of a minimum set of reporting criteria based on established single-EV flow cytometry reporting frameworks (Welsh et al., 2020f). One of the largest hurdles of multiplex analysis optimization is resolving the nonspecific binding of detection antibodies to beads. Ideally, a positive control method allowing identification of EVs, rather than just a nonspecifically bound antibody, to the beads could be identified, such as using a membrane dye. Such positive control (marker-positive) EVs are not generally available, and, to date, the authors have been unable to identify a suitable membrane dye that is compatible with the multiplex beads used in this study.

In summary, we have demonstrated that the use of stitched multiplex analysis in combination with MPA_{PASS} software is a powerful tool for creating, exploring, and analyzing data from hundreds of combinations of markers that can have great utility in guiding downstream quantitative single-EV methods or bulk EV subset analysis methods. This methodology holds utility for screening a large variety of markers simultaneously on EV-containing samples, with the main limitations being sample quantity and the semiquantitative nature of the assay itself. While super-resolution analysis (single-molecule detection) of single EVs is a highly quantitative assay with a demonstrated ability to identify clinical differences in samples, the clinical utility of such super-resolution assays is limited (Lennon et al., 2019; Tian et al., 2018) without robust EV repertoire assays. Stitched multiplex analyses, as performed with MPA_{PASS}, provide a means for EV repertoire analysis so that particular pathology-specific subsets can then be further quantified at a single-EV level as part of a systematic multiplex-to-single EV (MtSEA) pipeline. As such, MPA_{PASS} will streamline novel EV biomarker identification and the study of EV subset functions in health and disease.

STAR★METHODS

Detailed methods are provided in the online version of this paper and include the following:

- KEY RESOURCES TABLE
- RESOURCE AVAILABILITY
  - Lead contact
  - Materials availability
  - Data and code availability
- EXPERIMENTAL MODEL AND SUBJECT DETAILS
  - Ethics statement
- METHOD DETAILS
  - Human sample isolation and storage
  - EV isolation from human samples
  - FBS depletion of EVs
  - Cell culture
  - EV isolation from cell culture
  - Multiplex assay
  - Flow cytometry
  - Nanoparticle tracking analysis
  - MPA_{PASS} software
  - Normalization methods
- QUANTIFICATION AND STATISTICAL ANALYSIS
  - Limitations of the study

SUPPLEMENTAL INFORMATION

Supplemental information can be found online at https://doi.org/10.1016/j.crmeth.2021.100136.

ACKNOWLEDGMENTS

We thank the translational clinical programs and staff at the United States National Institutes of Health (NIH) National Cancer Institute (NCI) and the National Institute of Neurological Disorders and Stroke (NINDS) Clinics. J.W., T.T., B.K., J.K., J.S., J.L.G., J.B.T., M.M., T.G, T.C., C.H., A.A., H.M., M.L, K.C., J.G, A.L., J.B., E.R., K.A., and J.J. were supported by the Intramural Research Program of the NIH, NCI, Center for Cancer Research. S.J., S.M., and M.P. were supported by the intramural NIH, NINDS program. I.G., A.M., A.A-M., and J.J. were supported by the NIH Common Fund. J.J. specifically acknowledges NIH ZIA BC011502, ZIA BC011503, U01 HL126497, and UG3 TR002881, the Prostate Cancer Foundation, and the NCI-Curie Partnership Program (J.J. and C.T.). A.L. acknowledges NIH Z01-BC006161. F.R. was funded by the Deutsche Forschungsgemeinschaft (RI2616/3-1). A.I. acknowledges support by NIH 1R01GM120272 (A.I.) and R01CA218500 (A.I., I.G., and J.J.). J.W. is an International Society for Advancement of Cytometry (ISAC) Marylou Ingram Scholar (2019-2023).

AUTHOR CONTRIBUTIONS

J.A.W. and J.C.J. conceived this research and designed the experiments. All authors participated in sample and data acquisition, data analysis, and editing of the manuscript.

DECLARATION OF INTERESTS

A.G. has an affiliation with Evox Therapeutics, Ltd. All other authors declare no competing interests.

Received: February 11, 2021
Revised: August 31, 2021
Accepted: December 8, 2021
Published: January 24, 2022

REFERENCES

Gasecka, A., Nieuwland, R., Budnik, M., Dignat-George, F., Eyileten, C., Harrison, P., Lacroix, R., Leroyer, A., Opolski, G., Pluta, K., et al. (2020). Ticagrelor attenuates the increase of extracellular vesicle concentrations in plasma after acute myocardial infarction compared to clopidogrel. J. Thromb. Haemost. *18*, 609–623.

Issadore, D., Min, C., Liong, M., Chung, J., Weissleder, R., and Lee, H. (2011). Miniature magnetic resonance system for point-of-care diagnostics. Lab Chip *11*, 2282–2287.

Koliha, N., Wiencek, Y., Heider, U., Jungst, C., Kladt, N., Krauthauser, S., Johnston, I.C., Bosio, A., Schauss, A., and Wild, S. (2016). A novel multiplex bead-based platform highlights the diversity of extracellular vesicles. J. Extracell Vesicles *5*, 29975.

Lennon, K.M., Wakefield, D.L., Maddox, A.L., Brehove, M.S., Willner, A.N., Garcia-Mansfield, K., Meechoovet, B., Reiman, R., Hutchins, E., Miller, M.M., et al. (2019). Single molecule characterization of individual extracellular vesicles from pancreatic cancer. J. Extracell Vesicles *8*, 1685634.

Matsuzaki, J., and Ochiya, T. (2017). Circulating microRNAs and extracellular vesicles as potential cancer biomarkers: a systematic review. Int. J. Clin. Oncol. *22*, 413–420.

Murillo, O.D., Thistlethwaite, W., Rozowsky, J., Subramanian, S.L., Lucero, R., Shah, N., Jackson, A.R., Srinivasan, S., Chung, A., Laurent, C.D., et al. (2019). exRNA atlas analysis reveals distinct extracellular RNA cargo types and their carriers present across human biofluids. Cell *177*, 463–477.e15.

Reiner, A.T., Witwer, K.W., van Balkom, B.W.M., de Beer, J., Brodie, C., Corteling, R.L., Gabrielsson, S., Gimona, M., Ibrahim, A.G., de Kleijn, D., et al. (2017). Concise review: developing best-practice models for the therapeutic use of extracellular vesicles. Stem Cells Transl. Med *6*, 1730–1739.

Shao, H., Chung, J., Balaj, L., Charest, A., Bigner, D.D., Carter, B.S., Hochberg, F.H., Breakefield, X.O., Weissleder, R., and Lee, H. (2012). Protein typing of circulating microvesicles allows real-time monitoring of glioblastoma therapy. Nat. Med. *18*, 1835–1840.

Shao, H., Yoon, T.J., Liong, M., Weissleder, R., and Lee, H. (2010). Magnetic nanoparticles for biomedical NMR-based diagnostics. Beilstein J. Nanotechnol. *1*, 142–154.

Tertel, T., Bremer, M., Maire, C., Lamszus, K., Peine, S., Jawad, R., Andaloussi, S.E.L., Giebel, B., Ricklefs, F.L., and Gorgens, A. (2020). High-resolution imaging flow cytometry reveals impact of incubation temperature on labeling of extracellular vesicles with antibodies. Cytometry A *97*, 602–609.

Tian, Y., Gong, M., Hu, Y., Liu, H., Zhang, W., Zhang, M., Hu, X., Aubert, D., Zhu, S., Wu, L., and Yan, X. (2020). Quality and efficiency assessment of six extracellular vesicle isolation methods by nano-flow cytometry. J. Extracell Vesicles *9*, 1697028.

Tian, Y., Ma, L., Gong, M., Su, G., Zhu, S., Zhang, W., Wang, S., Li, Z., Chen, C., Li, L., et al. (2018). Protein profiling and sizing of extracellular vesicles from colorectal cancer patients via flow cytometry. ACS Nano *12*, 671–680.

van der Pol, E., Coumans, F., Varga, Z., Krumrey, M., and Nieuwland, R. (2013). Innovation in detection of microparticles and exosomes. J. Thromb. Haemost. *11*, 36–45.

van der Pol, E., Coumans, F.A., Grootemaat, A.E., Gardiner, C., Sargent, I.L., Harrison, P., Sturk, A., van Leeuwen, T.G., and Nieuwland, R. (2014). Particle size distribution of exosomes and microvesicles determined by transmission electron microscopy, flow cytometry, nanoparticle tracking analysis, and resistive pulse sensing. J. Thromb. Haemost. *12*, 1182–1192.

van der Pol, E., de Rond, L., Coumans, F.A.W., Gool, E.L., Boing, A.N., Sturk, A., Nieuwland, R., and van Leeuwen, T.G. (2018). Absolute sizing and label-free identification of extracellular vesicles by flow cytometry. Nanomedicine *14*, 801–810.

van der Pol, E., Hoekstra, A.G., Sturk, A., Otto, C., van Leeuwen, T.G., and Nieuwland, R. (2010). Optical and non-optical methods for detection and characterization of microparticles and exosomes. J. Thromb. Haemost. *8*, 2596–2607.

Welsh, J.A., Horak, P., Wilkinson, J.S., Ford, V.J., Jones, J.C., Smith, D., Holloway, J.A., and Englyst, N.A. (2020a). FCMPASS software aids extracellular vesicle light scatter standardization. Cytometry A *97*, 569–581.

Welsh, J.A., and Jones, J.C. (2020). Small particle fluorescence and light scatter calibration using FCMPASS software. Curr. Protoc. Cytometry *94*, e79.

Welsh, J.A., Jones, J.C., and Tang, V.A. (2020b). Fluorescence and light scatter calibration allow comparisons of small particle data in standard units across different flow cytometry platforms and detector settings. Cytometry A *97*, 592–601.

Welsh, J.A., Killingsworth, B., Kepley, J., Traynor, T., Mckinnon, K., Savage, J., Appel, D., Aldape, K., Camphausen, K., Berzofsky, J.A., et al. (2020c). A simple, high-throughput method of protein and label removal from extracellular vesicle samples. bioRxiv. https://doi.org/10.1039/D0NR07830A.

Welsh, J.A., Tang, V.A., van der Pol, E., and Gorgens, A. (2020d). MIFlowCyt-EV: the next chapter in the reporting and reliability of single extracellular vesicle flow cytometry experiments. Cytometry A *99A*, 365–368.

Welsh, J.A., van der Pol, E., Arkesteijn, G.J.A., Bremer, M., Brisson, A., Coumans, F., Dignat-George, F., Duggan, E., Ghiran, I., Giebel, B., and Gorgens, A. (2020e). MIFlowCyt-EV: a framework for standardized reporting of extracellular vesicle flow cytometry experiments. J. Extracell. Vesicles *9*, 1713526.

Welsh, J.A., van der Pol, E., Arkesteijn, G.J.A., Bremer, M., Brisson, A., Coumans, F., Dignat-George, F., Duggan, E., Ghiran, I., Giebel, B., et al. (2020f). MIFlowCyt-EV: a framework for standardized reporting of extracellular vesicle flow cytometry experiments. J. Extracell. Vesicles *9*, 1713526.

Wiklander, O.P.B., Bostancioglu, R.B., Welsh, J.A., Zickler, A.M., Murke, F., Corso, G., Felldin, U., Hagey, D.W., Evertsson, B., Liang, X.M., et al. (2018). Systematic methodological evaluation of a multiplex bead-based flow cytometry assay for detection of extracellular vesicle surface signatures. Front. Immunol. *9*, 1326.

Zhu, S., Ma, L., Wang, S., Chen, C., Zhang, W., Yang, L., Hang, W., Nolan, J.P., Wu, L., and Yan, X. (2014). Light-scattering detection below the level of single fluorescent molecules for high-resolution characterization of functional nanoparticles. ACS Nano *8*, 10998–11006.

STAR★METHODS

KEY RESOURCES TABLE

REAGENT or RESOURCE	SOURCE	IDENTIFIER
Antibodies		
CD9	Miltenyi Biotec	Cat# 130-108-813
CD63	Miltenyi Biotec	Cat# 130-108-813
CD81	Miltenyi Biotec	Cat# 130-108-813
CTLA-4	BioLegend	Cat# 369612; RRID: AB_2632873
CD166	Miltenyi Biotec	Cat# 130-106-576; RRID: AB_2655529
CD147	BioLegend	Cat# 306214; RRID: AB_2750170
CD87	Miltenyi Biotec	Cat# 130-114-851; RRID: AB_2726804
CD90	BioLegend	Cat# 328114; RRID: AB_893431
CD47	BioLegend	Cat# 323124; RRID: AB_2716203
CD38	BioLegend	Cat# 303510; RRID: AB_314362
CD15	BioLegend	Cat# 301908; RRID: AB_314200
CD171	Miltenyi Biotec	Cat# 130-100-684; RRID: AB_2655584
CD49F	BioLegend	Cat# 313616; RRID: AB_1575047
VEGFR	Miltenyi Biotec	Cat# 130-093-601; AB_10828920
EGFR	BioLegend	Cat# 352906; AB_11150410
EGFRvIII	Novus Biologicals	Cat# NBP2-50599AF647; RRID: AB_2904021
CD140	BioLegend	Cat# 323608; RRID: AB_2162787
CD10	Miltenyi Biotec	Cat# 130-093-450; RRID: AB_10828545
CA9	Miltenyi Biotec	Cat# 130-110-058; RRID: AB_2651327
CD314	BioLegend	Cat# 320808; RRID: AB_492962
Biological samples		
Human cerebral spinal fluid	National Institutes of Health (Dr. Steven Jacobson, Dr. Jennifer Jones)	N/A
Human plasma and serum	National Institutes of Health (Dr. Steven Jacobson, Dr. Jennifer Jones)	N/A
Chemicals, peptides, and recombinant proteins		
Dulbecco Phosphate Buffered Saline	ThermoFisher Scientific	14190144
RPMI 1640 Medium	ThermoFisher Scientific	11875093
RPMI 1640 Medium (no phenol red)	ThermoFisher Scientific	11835030
McCoy's 5A (Modified) Medium	ThermoFisher Scientific	16600082
Critical commercial assays		
MACSPlex Exosome Kit, human	Miltenyi Biotec	130-108-813
Deposited data		
Example database	This publication	https://doi.org/10.5281/zenodo.5725951
Experimental models: Cell lines		
PC3	Laboratory of Hisataka Kobayashi, NCI, NIH	N/A
PC3pip	Laboratory of Hisataka Kobayashi, NCI, NIH	N/A
U87	Laboratory of Kevin Camphausen, NCI, NIH	N/A
U251	Laboratory of Kevin Camphausen, NCI, NIH	N/A
HCT116 wt	Laboratory of Curt Harris, NCI, NIH	N/A
HCT116 mt	Laboratory of Curt Harris, NCI, NIH	N/A
HCT116 -/-	Laboratory of Curt Harris, NCI, NIH	N/A

(*Continued on next page*)

Continued

REAGENT or RESOURCE	SOURCE	IDENTIFIER
UOK111	Laboratory of W. Marston Linehan, NCI, NIH	N/A
UOK151	Laboratory of W. Marston Linehan, NCI, NIH	N/A
Software and algorithms		
MATLAB	Mathworks, Inc	https://www.mathworks.com/
MPA_{PASS} Software	NIH	Original Code https://zenodo.org/record/5725534#.YZ7r-b3MIUE Standalone Software https://nano.ccr.cancer.gov/mpapass/
Other		
qEVOriginal 70 nm	Izon Biosciences	N/A
qEV-10 70 nm	Izon Biosciences	N/A
JumboSep	PALL Corporation	FD100K65
Nanosight LM10	Malvern	N/A
CytoFLEX S	Beckman Coulter	N/A
Aurora	Cytek Biosciences	N/A
Optima XE ultracentrifuge	Beckman Coulter	B10049
45 titanium rotor	Beckman Coulter	339160

RESOURCE AVAILABILITY

Lead contact

Requests for further information and requests for resources or reagents in this manuscript should be directed to the lead contact author, Jennifer Jones (jennifer.jones2@nih.gov).

Materials availability

No unique reagents were generated in this study.

Data and code availability

- Multiplex data has been shared in Supplementary Data 1. Any further data reported in this paper will be shared by the lead contact upon request.
- All original code has been deposited at Zenodo and is publicly available as of the date of publication. https://doi.org/10.5281/zenodo.5725533
- Any additional information for reanalysis of the data reported in this paper may be requested from the lead contact.

EXPERIMENTAL MODEL AND SUBJECT DETAILS

Ethics statement

Serum, plasma, and CSF samples used in this study were collected from the subject followed at the National Institute of Neurologic Disorders and Stroke under protocols # 98-N-0047, 89-N-0045, 13-N-0017, 13-N-0149. Prior to study inclusion, written informed consent was obtained from all subjects in accordance with the Declaration of Helsinki. Sample metadata for donors can be found in data database (see key resources table). Further statistical analysis of biofluid data was not performed, as the samples were de-identified, and age and sex information was not available for this study. Cell line models (PC3, PC3pip, U87, U251, UOK111, UOK151, HCT116 wt, HCT116 mt, HCT116 −/−) were used to produce EVs. Further details on culture conditions and source can be found in 'STAR Methods' and the 'key resources table', respectively.

METHOD DETAILS

Human sample isolation and storage

CSF samples were obtained by lumbar puncture. After centrifugation at 1,300×*g* for 10 minutes, the supernatants were collected into cryotubes and immediately frozen at −80°C until use. Whole blood was collected using serum separation tubes and centrifuged at 2000×*g* for 10 minutes. After centrifugation, the supernatants were collected into cryotubes and immediately frozen at −80°C until use. Plasma samples were collected in EDTA vacutainers. Samples were centrifuged at 900×*g* for 7 minutes. After centrifugation, the

supernatants were collected into cryotubes and immediately frozen at −80°C until use. All samples were thawed at 37°C for 10 minutes. Plasma samples were centrifuged at 2500×*g* for 10 minutes twice to remove residual platelets.

EV isolation from human samples

Platelet-poor plasma (PPP) samples were created by centrifuging 2 mL of plasma twice at 2000×*g* for 10 minutes twice with the supernatant isolated. Multiplex samples referred to as 'neat' were aliquoted from PPP into multiplex bead mixture in the volumes outlined in the database (see key resources table) and results sections. EVs isolated from PPP using size exclusion chromatography (qEV-5, Izon Bioscience) were performed by adding 500 μL to the top of a qEV with fractions collected in 500 μL volumes. Fraction 7–9 were pooled, and the volumes incubated with multiplex beads are outlined in the database (see key resources table) and results sections. EV-Clean, a multimodal resin composition, in this case CaptoCore 700 (Cytiva Life Sciences, Cat. 17548101), prepared EVs were created by incubating 50 μL of PPP with 100 μL of resin for 30 minutes at room temperature, as previously described (Welsh et al., 2020c). The supernatant was removed from the resin and incubated with multiplex beads in the volumes indicated within the database (see key resources table) and results sections. 2 mL of CSF was concentrated to ∼50 μL using 100 kDa filters (Nanosep, PALL, Cat. OD100C34).

FBS depletion of EVs

To deplete FBS of EVs, 13 mL of fetal bovine serum (FBS) was added to 52 mL cell line media and added to a 65 mL ultracentrifugation tube. Tubes were placed in a pre-cooled 45 titanium (Ti) rotor and centrifuged at 100,000×*g* (k-factor 312.6) for 18 hours at 4°C using an Optima XE centrifuge (Beckman Coulter). The top 50 mL of supernatant from each tube was immediately removed and added to an equal volume of media to create a 10% EV-depleted FBS media stock.

Cell culture

PC3 and PC3pip cell lines were cultured in ∼35 mL 0.22 μm-filtered, phenol red, RPMI-1640, 10% EV-depleted FBS, 1% Pen/Strep, and 1% L-glutamine. HCT116 wild-type (wt), HCT116 p53 knock-out (−/−), and HCT116 mutant (mt) lines were cultured in ∼35 mL 0.22 μm-filtered, phenol red, McCoy's modified medium, 10% EV-depleted FBS, 1% Pen/Strep, and 1% L-glutamine. Cell lines were cultured in Falcon T175 tissue culture flasks with ambient (21%) oxygen and 5% CO2. U87 and U251 cell lines were cultured in Dulbecco-modified Eagle medium, with 4.5 mg mL^{-1} glucose, L-glutamine, 110 mg L^{-1} sodium pyruvate, 10% FBS. U87 and U251 cell lines were cultured in hypoxic conditions with 5% oxygen. Prior to EV collection cell lines were transferred to phenol red free media with 10% EV-depleted FBS for 24–48 hours.

EV isolation from cell culture

EV containing cell culture supernatants were aspirated from tissue culture flasks and transferred to 50 mL tubes. The tubes were centrifuged in 50 mL aliquots at 2000×*g* twice for 10 minutes. Cell-free supernatant was aliquoted into 60 mL JumboSep canisters (PALL Corporation) and concentrated using 100 kDa filters (JumboSep, PALL Corporation) until ∼5 mL was left. The 5 mL of cell-free concentrate was then run on a 10 mL 70 nm size exclusion column (qEV, Izon Science) with 5 mL fractions collected. The first 15 fractions were collected starting immediately after the sample was pipetted onto the column. EV concentration and protein content of fractions were approximated using nanoparticle tracking analysis (LM10, Malvern) and NanoDrop (Thermo Fisher Scientific), respectively, Figure S1. Fractions 7–9 of each preparation were mixed and used for multiplex experiments.

Multiplex assay

EVs were incubated with 15 μL of MACSPlex Exosome Kit (Miltenyi Biotec, Cat No. 130-108-813) in 500 μL low protein binding tubes overnight at 21°C and protected from light. EV inputs were based on total particle numbers obtained using NTA. The total counts of particles incubated are outlined for each figure. A 1.2 μm filter plate was washed using 150 μL of MACSPlex buffer (Miltenyi Biotec) and cleared using a vacuum manifold. Experiments comparing blocking buffers replaced MACSPlex buffer at all steps with 2% EV-depleted FBS. FBS depletion of EVs was described previously, with the 10% resulting stock diluted to 2% with Dulbecco phosphate buffered saline (Gibco, Cat. No. 14190144). 50 μL of MACSPlex (Miltenyi Biotec) buffer was added to each well before incubated EV-capture bead mixture was aliquoted into each of the wells. The EV-capture bead mixture was washed using vacuum manifold and immediately resuspended in 150 μL buffer to each well. Wells were reverse pipetted to resuspend beads. Antibody (information including volume, concentration, manufacturers, catalogue numbers can be found in Table 1 and respective MPA_{PASS} .xls database files for each assay) was then added to each well and incubated, protected from light and shaking, for two hours at room temperature. Samples were reverse pipetted before washing using the vacuum manifold and immediately resuspending in 150 μL MACSPlex buffer, this was repeated. Each well was resuspended with 75 μL MACSPlex buffer, reverse pipetted and transferred to 96-well V-bottom polypropylene plates. This was repeated to ensure maximal bead recovery from the 1.2 μm filter plates, giving a final volume of 150 μL. Samples were then analyzed using flow cytometry. A detailed protocol and template for applying the multiplex samples to cell culture EVs can be found in Methods S1) and at: https://doi.org/10.17504/protocols.io.be7yjhpw;

Flow cytometry

Beads were triggered using a forward light scatter threshold and optimal gains for each detector (CytoFLEX S, Beckman Coulter, USA; Aurora, Cytek Bioscience, USA) were found by performing voltration on 8-peak beads (Cat. 422903, BioLegend, USA). A detailed protocol for bead gating strategies using FlowJo Software can be found in Methods S2 and at: https://doi.org/10.17504/protocols.io.bm3gk8jw. Briefly, Figure 1 outlines the types of signal that can originate from the multiplex assays (Figure 1A), shows how singlets are gated (Figure 1B), and the fluorescent 'bar-coding' of the multiplex array (Figure 1C) and the specificity of each population (Figure 1D).

Nanoparticle tracking analysis

Detectable sample concentration was approximated using a NanoSight LM10 instrument (Malvern, UK), equipped with a 405 nm LM12 module and EMCCD camera (DL-658-OEM-630, Andor). Video acquisition was performed with NTA software v3.4, using a camera level of 14. Three 30 second videos were captured per sample. Post-acquisition video analysis used the following settings: minimum track length = 5, detection threshold = 4, automatic blur size = 2-pass, maximum jump size = 12.0. Exported datasets were compiled and plotted using scripts written in MATLAB (v9.7.0.1261785 (R2019b) Update 3, The Mathworks Inc, Natick, MA).

MPA_{PASS} software

A standalone software package for multiplex analysis was developed using MATLAB (v9.7.0.1261785 (R2019b) Update 3, The Mathworks Inc, Natick, MA). Compiled standalone software and GitHub repository links are available from nanopass.ccr.cancer.gov/mpapass. Maintained protocols for the use of the software can be found at: https://doi.org/10.17504/protocols.io.bm3gk8jw. An example import database for the software can be found at the "example database" link provided in the key resources table.

Normalization methods

Normalization methods shown in Figure 1C are as shown below and named separation index 1 and 2 (SI1-2), fold change (FC), and background subtraction (BS). Each method uses the median of positive bead, $\tilde{y}$, and negative bead, $\tilde{x}$. All methods are available for use within the MPA_{PASS} package. Results in the manuscript used fold-change to avoid the creation of negative numbers thereby allowing logarithmic transformation of data for conducting downstream analyses without the need to alter or exclude datapoints.

$$SI1 = \frac{\tilde{y} - \tilde{x}}{x_{95\%}}$$

$$SI2 = \frac{\tilde{y} - \tilde{x}}{(x_{95\%} - \tilde{x}) + (y_{5\%} + \tilde{y})}$$

$$FC = \frac{\tilde{y}}{\tilde{x}}$$

$$BS = \tilde{y} - \tilde{x}$$

QUANTIFICATION AND STATISTICAL ANALYSIS

Multiplex data was analyzed using MPA_{PASS} software, normalization methods are noted in figure legends and formulas used can be found in 'normalization methods' section of STAR Methods.

Limitations of the study

Despite being a powerful method to identify markers useful for immune-affinity isolation methods or downstream single particle analysis, multiplex analysis itself is semi-quantitative and the changes in signal intensity can occur for a variety of reasons. For this reason, statistical analysis methods using post-hoc tests have been excluded from the MPA_{PASS} software, which has been designed to primarily inspect data quality; stitch, normalize, and explore large multiplex dataset; perform data-reduction methods; and semi-qualitatively identify markers and associations that appear between samples.

Cell Reports Methods, Volume *2*

Supplemental information

MPA_{PASS} software enables stitched multiplex, multidimensional EV repertoire analysis and a standard framework for reporting bead-based assays

Joshua A. Welsh, Bryce Killingsworth, Julia Kepley, Tim Traynor, Sean Cook, Jason Savage, Jenn Marte, Min-Jung Lee, Hoyoung M. Maeng, Michelle L. Pleet, Setty Magana, André Gorgens, Cecile L. Maire, Katrin Lamszus, Franz L. Ricklefs, Maria J. Merino, W. Marston Linehan, Tim Greten, Tomer Cooks, Curtis C. Harris, Andrea Apolo, Asim Abdel-Mageed, Alexander R. Ivanov, Jane B. Trepel, Matthew Roth, Mercedes Tkach, Aleksandar Milosavljevic, Clotilde Théry, Amy LeBlanc, Jay A. Berzofsky, Eytan Ruppin, Kenneth Aldape, Kevin Camphausen, James L. Gulley, Ionita Ghiran, Steve Jacobson, and Jennifer C. Jones

Figure S1. EV and protein concentration across qEV fractions. Overlaid on the elution fraction particle and protein concentration curves is a representative diameter distribution of each of the EV containing fractions used for the downstream multiplex analysis. Related to Figure 2 & 3.

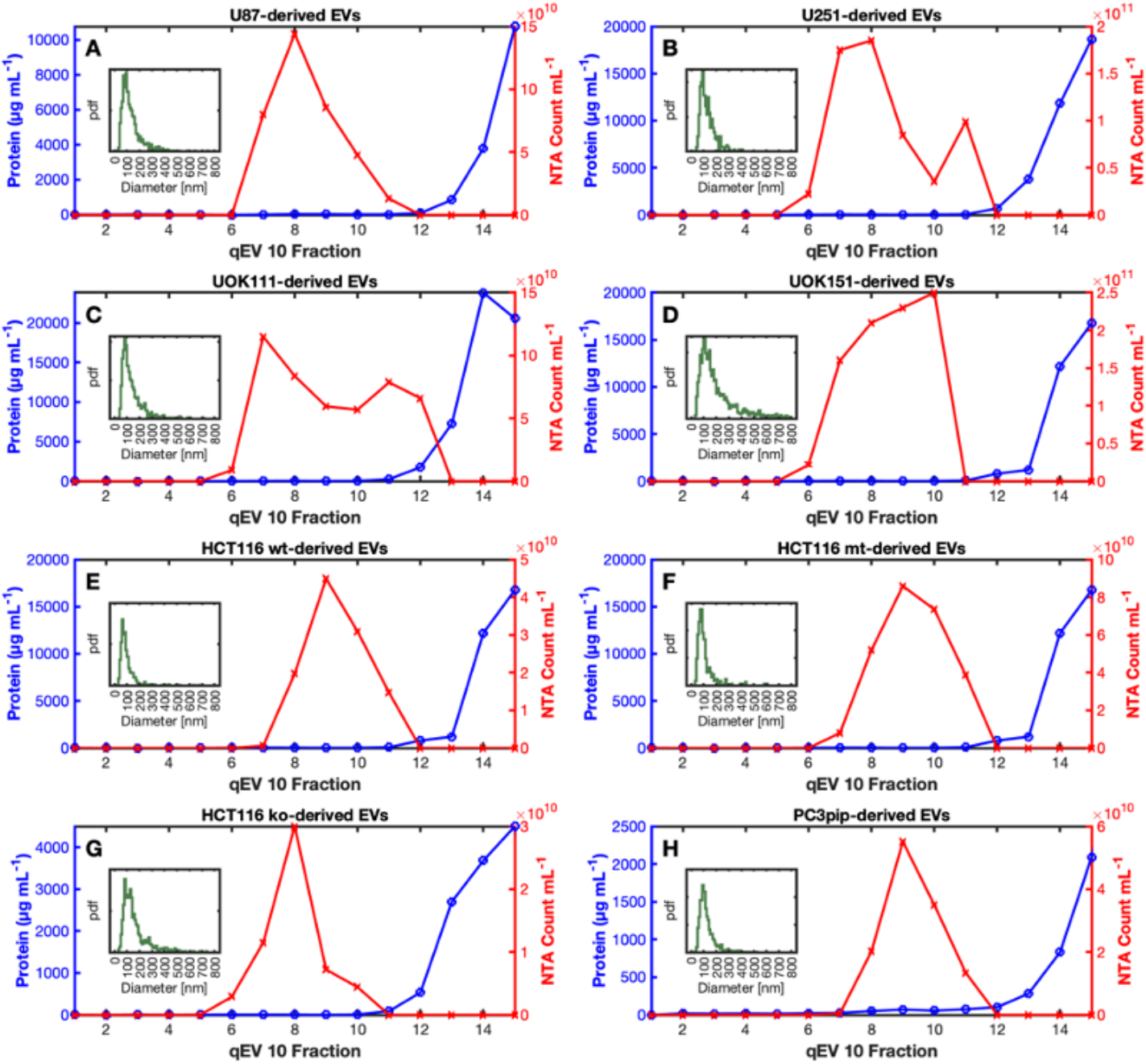
A
U87-derived EVs
B
U251-derived EVs
C
UOK111-derived EVs
D
UOK151-derived EVs
E
HCT116 wt-derived EVs
F
HCT116 mt-derived EVs
G
HCT116 ko-derived EVs
H
PC3pip-derived EVs
Protein (µg mL-1)
NTA Count mL-1
qEV 10 Fraction
pdf
Diameter [nm]

Figure S2. Multiplex input titration. Titration of two different cell line derived EVs from $1x10^6$ to $1x10^{10}$ total EVs. Scatter plots (bottom) showing the titration of total U87- and PC3pip-derived EVs when incubated with multiplex array. Intensities are of EV mix (CD9, CD63, CD81) and shown for a subset of capture beads (CD81, CD63, CD44, and CD29). Data was normalized using fold change. Related to Figure 2.

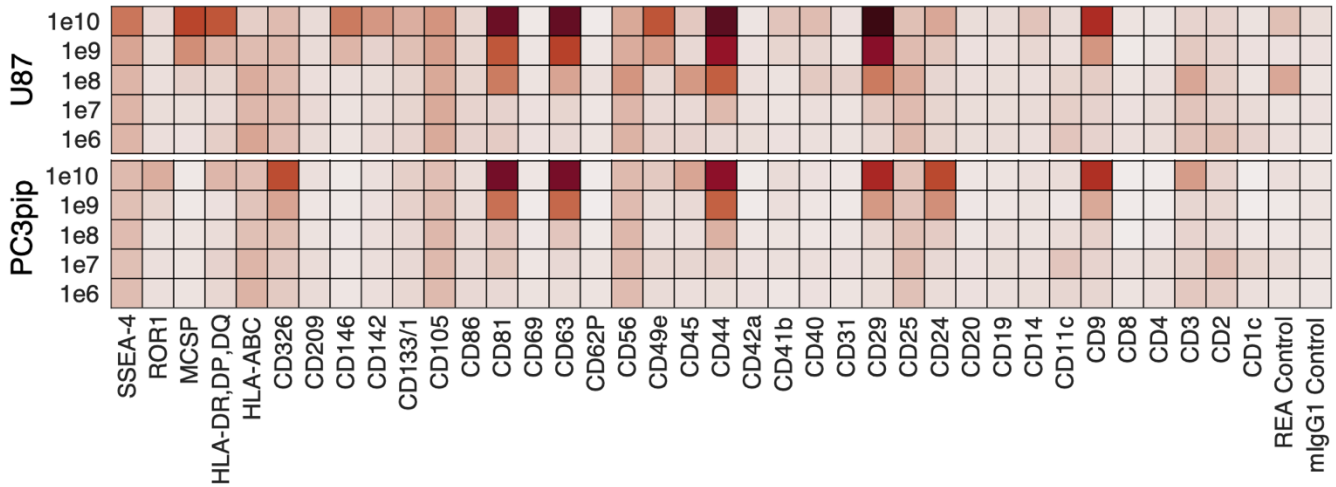
U87
PC3pip
1e10
1e9
1e8
1e7
1e6
SSEA-4
ROR1
MCSP
HLA-DR,DP,DQ
HLA-ABC
CD326
CD209
CD146
CD142
CD133/1
CD105
CD86
CD81
CD69
CD63
CD62P
CD56
CD49e
CD45
CD44
CD42a
CD41b
CD40
CD31
CD29
CD25
CD24
CD20
CD19
CD14
CD11c
CD9
CD8
CD4
CD3
CD2
CD1c
REA Control
mIgG1 Control

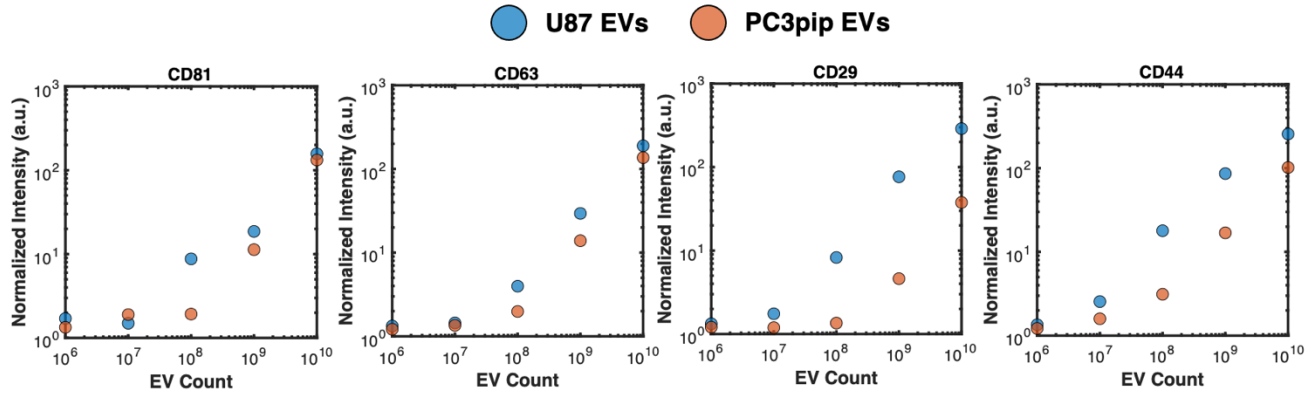
U87 EVs
PC3pip EVs
CD81
CD63
CD29
CD44
Normalized Intensity (a.u.)
EV Count

Figure S3. Screening antibodies for non-specific binding. All capture beads when incubated with 0.5 µg of detection antibody with buffer (asterixis markers) were incubated as negative controls. EV samples derived from U87 (circle marker) and U251 (square marker) cell lines were used as positive controls. The included Miltenyi buffer (red markers) and 2% EV-depleted FBS (black markers) were also compared. Related to Figure 3.

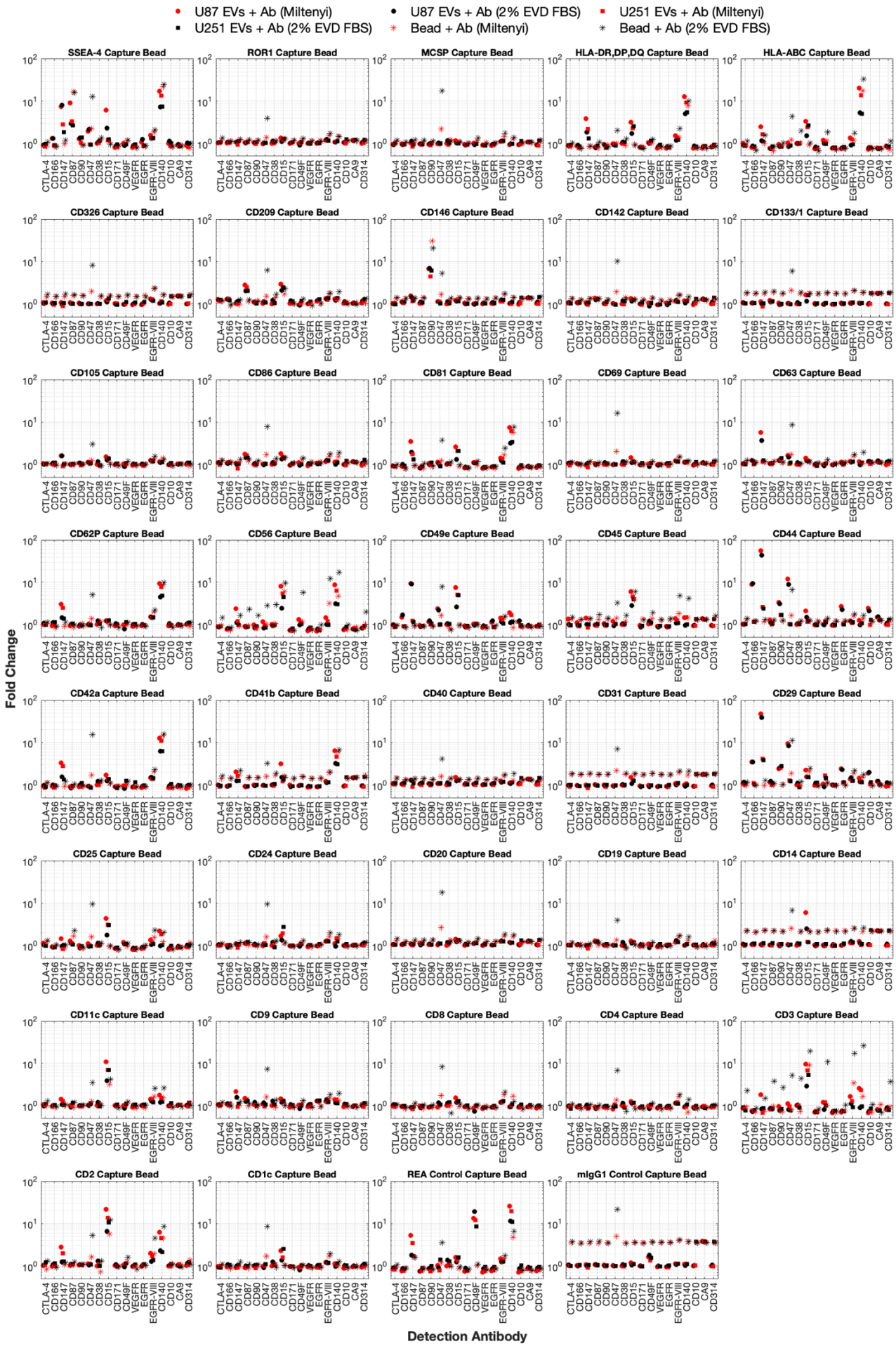
U87 EVs + Ab (Miltenyi)
U87 EVs + Ab (2% EVD FBS)
U251 EVs + Ab (Miltenyi)
U251 EVs + Ab (2% EVD FBS)
Bead + Ab (Miltenyi)
Bead + Ab (2% EVD FBS)
SSEA-4 Capture Bead
ROR1 Capture Bead
MCSP Capture Bead
HLA-DR,DP,DQ Capture Bead
HLA-ABC Capture Bead
CD326 Capture Bead
CD209 Capture Bead
CD146 Capture Bead
CD142 Capture Bead
CD133/1 Capture Bead
CD105 Capture Bead
CD86 Capture Bead
CD81 Capture Bead
CD69 Capture Bead
CD63 Capture Bead
CD62P Capture Bead
CD56 Capture Bead
CD49e Capture Bead
CD45 Capture Bead
CD44 Capture Bead
CD42a Capture Bead
CD41b Capture Bead
CD40 Capture Bead
CD31 Capture Bead
CD29 Capture Bead
CD25 Capture Bead
CD24 Capture Bead
CD20 Capture Bead
CD19 Capture Bead
CD14 Capture Bead
CD11c Capture Bead
CD9 Capture Bead
CD8 Capture Bead
CD4 Capture Bead
CD3 Capture Bead
CD2 Capture Bead
CD1c Capture Bead
REA Control Capture Bead
mIgG1 Control Capture Bead
Fold Change
Detection Antibody
CTLA-4
CD166
CD147
CD87
CD90
CD47
CD38
CD15
CD171
CD49F
VEGFR
EGFR
EGFR-VIII
CD140
CD10
CA9
CD314

Figure S4. Screening antibodies for non-specific binding using hierarchal clustering. A) Boxplot comparing the top 75 average bead intensities combinations across U87-derived EVs, U251-derived EVs, and bead + antibody controls. Phenotypes are order by detection antibody followed by capture antibody e.g. CD140 detection, SSEA-4 capture. **B)** heatmap showing hierarchically clustered raw data of U87-derived EVs, U251-derived EVs, and bead + antibody controls intensities. Related to Figure 3.

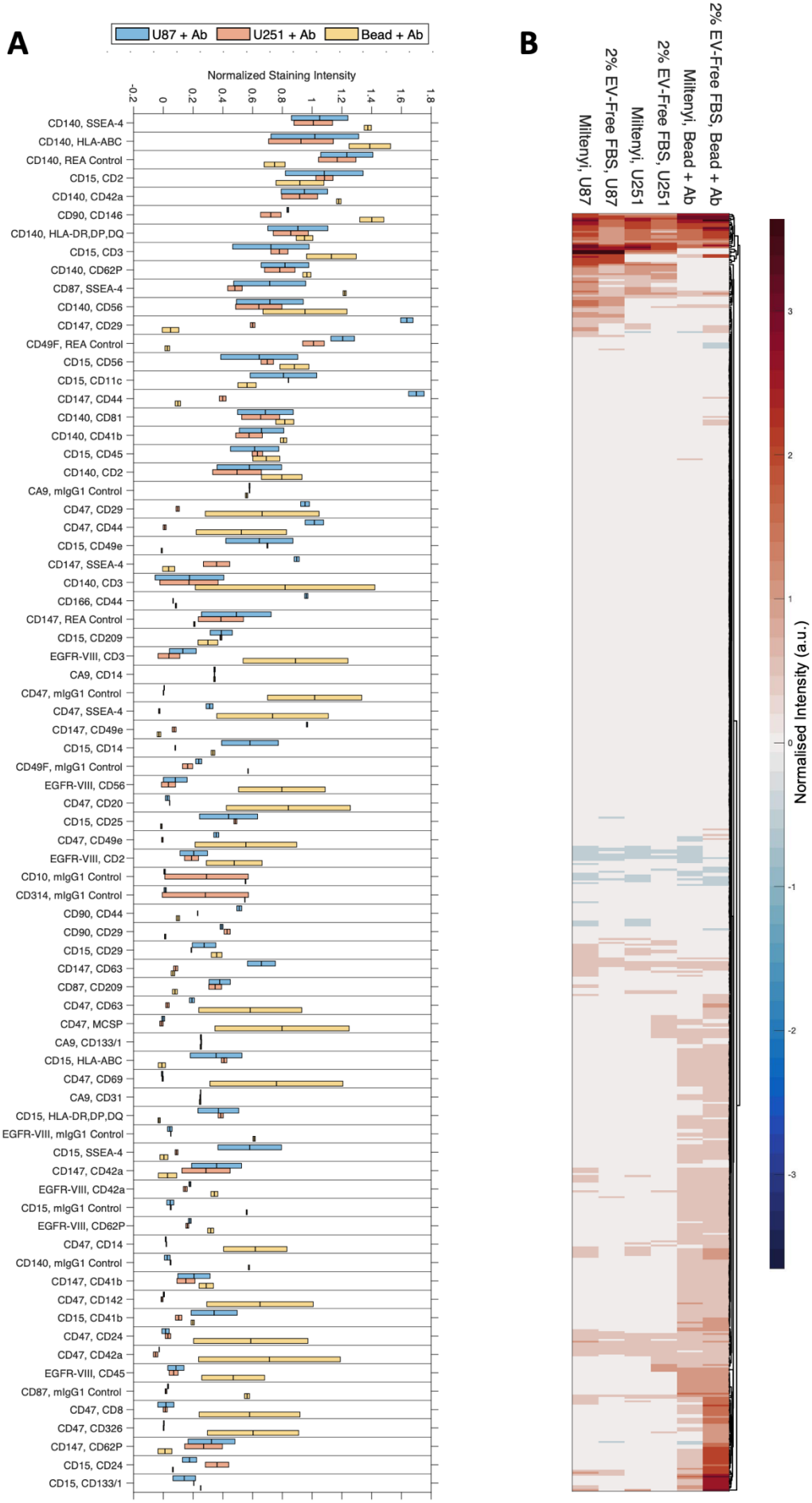
A
U87 + Ab
U251 + Ab
Bead + Ab
Normalized Staining Intensity
-0.2
0
0.2
0.4
0.6
0.8
1
1.2
1.4
1.6
1.8
CD140, SSEA-4
CD140, HLA-ABC
CD140, REA Control
CD15, CD2
CD140, CD42a
CD90, CD146
CD140, HLA-DR,DP,DQ
CD15, CD3
CD140, CD62P
CD87, SSEA-4
CD140, CD56
CD147, CD29
CD49F, REA Control
CD15, CD56
CD15, CD11c
CD147, CD44
CD140, CD81
CD140, CD41b
CD15, CD45
CD140, CD2
CA9, mIgG1 Control
CD47, CD29
CD47, CD44
CD15, CD49e
CD147, SSEA-4
CD140, CD3
CD166, CD44
CD147, REA Control
CD15, CD209
EGFR-VIII, CD3
CA9, CD14
CD47, mIgG1 Control
CD47, SSEA-4
CD147, CD49e
CD15, CD14
CD49F, mIgG1 Control
EGFR-VIII, CD56
CD47, CD20
CD15, CD25
CD47, CD49e
EGFR-VIII, CD2
CD10, mIgG1 Control
CD314, mIgG1 Control
CD90, CD44
CD90, CD29
CD15, CD29
CD147, CD63
CD87, CD209
CD47, CD63
CD47, MCSP
CA9, CD133/1
CD15, HLA-ABC
CD47, CD69
CA9, CD31
CD15, HLA-DR,DP,DQ
EGFR-VIII, mIgG1 Control
CD15, SSEA-4
CD147, CD42a
EGFR-VIII, CD42a
CD15, mIgG1 Control
EGFR-VIII, CD62P
CD47, CD14
CD140, mIgG1 Control
CD147, CD41b
CD47, CD142
CD15, CD41b
CD47, CD24
CD47, CD42a
EGFR-VIII, CD45
CD87, mIgG1 Control
CD47, CD8
CD47, CD326
CD147, CD62P
CD15, CD24
CD15, CD133/1
B
2% EV-Free FBS, Bead + Ab
Miltenyi, Bead + Ab
2% EV-Free FBS, U251
Miltenyi, U251
2% EV-Free FBS, U87
Miltenyi, U87
3
2
1
0
-1
-2
-3
Normalised Intensity (a.u.)

Figure S5. Identifying marker differences between biological fluids. A) Heatmap shows a high-level overview of hierarchically clustered samples and markers from samples of plasma, serum, and CSF stained when incubated with CD9, CD63, and CD81 independently across 39 unique capture beads and stitched analysis is applied. **B)** shows a selection of the heatmap where markers within CSF appear to be enriched when compared to plasma and serum. Related to Figure 4.

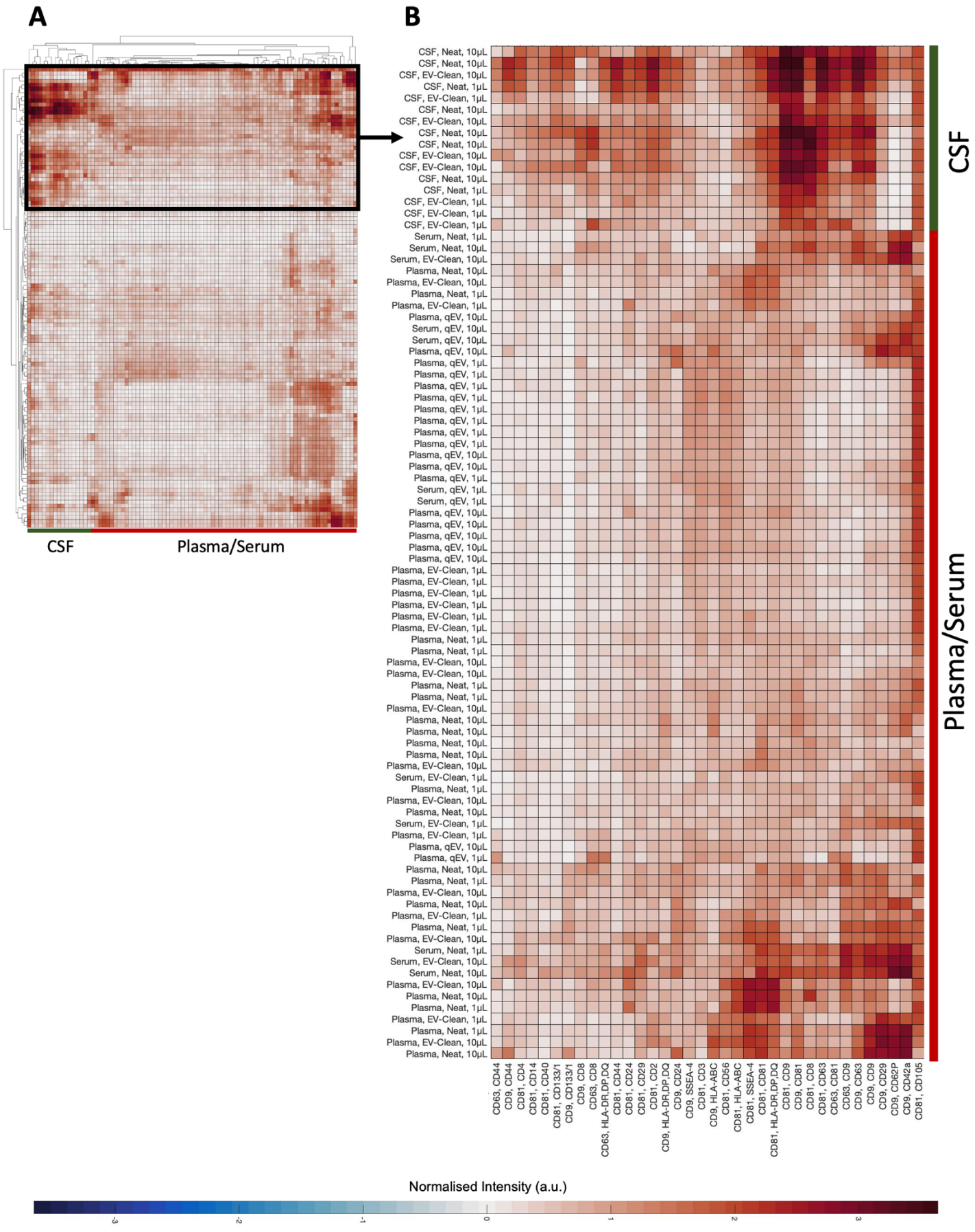
A
B
CSF
Plasma/Serum
CSF, Neat, 10µL
CSF, Neat, 10µL
CSF, EV-Clean, 10µL
CSF, Neat, 1µL
CSF, EV-Clean, 1µL
CSF, Neat, 10µL
CSF, EV-Clean, 10µL
CSF, Neat, 10µL
CSF, Neat, 10µL
CSF, EV-Clean, 10µL
CSF, EV-Clean, 10µL
CSF, Neat, 10µL
CSF, Neat, 1µL
CSF, EV-Clean, 1µL
CSF, EV-Clean, 1µL
CSF, EV-Clean, 1µL
Serum, Neat, 1µL
Serum, Neat, 10µL
Serum, EV-Clean, 10µL
Plasma, Neat, 10µL
Plasma, EV-Clean, 10µL
Plasma, Neat, 1µL
Plasma, EV-Clean, 1µL
Plasma, qEV, 10µL
Serum, qEV, 10µL
Serum, qEV, 10µL
Plasma, qEV, 10µL
Plasma, qEV, 1µL
Plasma, qEV, 1µL
Plasma, qEV, 1µL
Plasma, qEV, 1µL
Plasma, qEV, 1µL
Plasma, qEV, 1µL
Plasma, qEV, 1µL
Plasma, qEV, 1µL
Plasma, qEV, 10µL
Plasma, qEV, 10µL
Plasma, qEV, 1µL
Serum, qEV, 1µL
Serum, qEV, 1µL
Plasma, qEV, 10µL
Plasma, qEV, 10µL
Plasma, qEV, 10µL
Plasma, qEV, 10µL
Plasma, qEV, 10µL
Plasma, EV-Clean, 1µL
Plasma, EV-Clean, 1µL
Plasma, EV-Clean, 1µL
Plasma, EV-Clean, 1µL
Plasma, EV-Clean, 1µL
Plasma, EV-Clean, 1µL
Plasma, Neat, 1µL
Plasma, Neat, 1µL
Plasma, EV-Clean, 10µL
Plasma, EV-Clean, 10µL
Plasma, Neat, 1µL
Plasma, Neat, 1µL
Plasma, EV-Clean, 10µL
Plasma, Neat, 10µL
Plasma, Neat, 10µL
Plasma, Neat, 10µL
Plasma, Neat, 10µL
Plasma, EV-Clean, 10µL
Serum, EV-Clean, 1µL
Plasma, Neat, 1µL
Plasma, EV-Clean, 10µL
Plasma, Neat, 10µL
Serum, EV-Clean, 1µL
Plasma, EV-Clean, 1µL
Plasma, qEV, 10µL
Plasma, qEV, 1µL
Plasma, Neat, 10µL
Plasma, Neat, 1µL
Plasma, EV-Clean, 10µL
Plasma, Neat, 10µL
Plasma, EV-Clean, 1µL
Plasma, Neat, 1µL
Plasma, EV-Clean, 10µL
Serum, Neat, 1µL
Serum, EV-Clean, 10µL
Serum, Neat, 10µL
Plasma, EV-Clean, 10µL
Plasma, Neat, 10µL
Plasma, Neat, 1µL
Plasma, EV-Clean, 1µL
Plasma, Neat, 1µL
Plasma, EV-Clean, 10µL
Plasma, Neat, 10µL
CD63, CD44
CD9, CD44
CD81, CD4
CD81, CD14
CD81, CD40
CD81, CD133/1
CD9, CD133/1
CD9, CD8
CD63, CD8
CD63, HLA-DR,DP,DQ
CD81, CD44
CD81, CD24
CD81, CD29
CD81, CD2
CD9, HLA-DR,DP,DQ
CD9, CD24
CD9, SSEA-4
CD81, CD3
CD9, HLA-ABC
CD81, CD56
CD81, HLA-ABC
CD81, SSEA-4
CD81, CD81
CD81, HLA-DR,DP,DQ
CD81, CD9
CD9, CD81
CD81, CD8
CD81, CD63
CD63, CD81
CD63, CD9
CD9, CD63
CD9, CD9
CD9, CD29
CD9, CD62P
CD9, CD42a
CD81, CD105
CSF
Plasma/Serum
Normalised Intensity (a.u.)
-3
-2
-1
0
1
2
3

Figure S6 – Matched timepoint comparison of samples obtained from single individual with Streck, EDTA, Serum, Serum-Activated blood isolation tubes. Samples were incubated with a total count of $1x10^9$ or $1x10^{10}$ EVs either neat or post-qEV column. Due to it not being possible to count EVs from neat biological fluids without counting other particles, concentrations were assumed to be ~5-fold diluted by using the qEV column. Related to Figure 4.

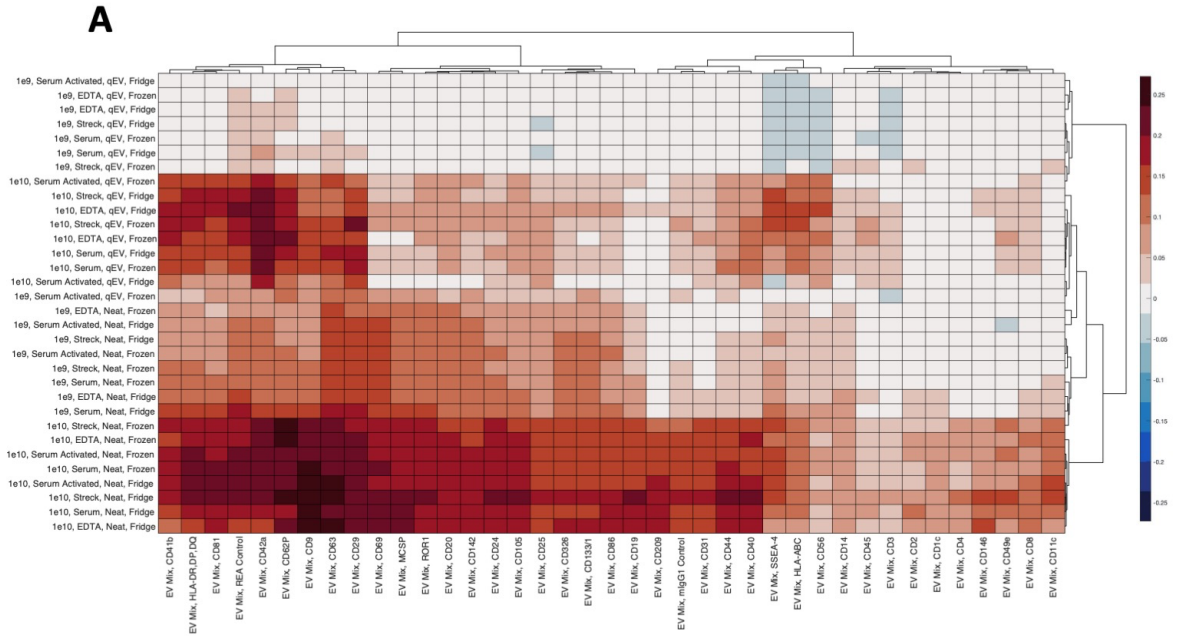
A
1e9, Serum Activated, qEV, Fridge
1e9, EDTA, qEV, Frozen
1e9, EDTA, qEV, Fridge
1e9, Streck, qEV, Fridge
1e9, Serum, qEV, Frozen
1e9, Serum, qEV, Fridge
1e9, Streck, qEV, Frozen
1e10, Serum Activated, qEV, Frozen
1e10, Streck, qEV, Fridge
1e10, EDTA, qEV, Fridge
1e10, Streck, qEV, Frozen
1e10, EDTA, qEV, Frozen
1e10, Serum, qEV, Fridge
1e10, Serum, qEV, Frozen
1e10, Serum Activated, qEV, Fridge
1e9, Serum Activated, qEV, Frozen
1e9, EDTA, Neat, Frozen
1e9, Serum Activated, Neat, Fridge
1e9, Streck, Neat, Fridge
1e9, Serum Activated, Neat, Frozen
1e9, Streck, Neat, Frozen
1e9, Serum, Neat, Frozen
1e9, EDTA, Neat, Fridge
1e9, Serum, Neat, Fridge
1e10, Streck, Neat, Frozen
1e10, EDTA, Neat, Frozen
1e10, Serum Activated, Neat, Frozen
1e10, Serum, Neat, Frozen
1e10, Serum Activated, Neat, Fridge
1e10, Streck, Neat, Fridge
1e10, Serum, Neat, Fridge
1e10, EDTA, Neat, Fridge
EV Mix, CD41b
EV Mix, HLA-DR,DP,DQ
EV Mix, CD81
EV Mix, REA Control
EV Mix, CD42a
EV Mix, CD62P
EV Mix, CD9
EV Mix, CD63
EV Mix, CD29
EV Mix, CD69
EV Mix, MCSP
EV Mix, ROR1
EV Mix, CD20
EV Mix, CD142
EV Mix, CD24
EV Mix, CD105
EV Mix, CD25
EV Mix, CD326
EV Mix, CD133/1
EV Mix, CD86
EV Mix, CD19
EV Mix, CD209
EV Mix, mIgG1 Control
EV Mix, CD31
EV Mix, CD44
EV Mix, CD40
EV Mix, SSEA-4
EV Mix, HLA-ABC
EV Mix, CD56
EV Mix, CD14
EV Mix, CD45
EV Mix, CD3
EV Mix, CD2
EV Mix, CD1c
EV Mix, CD4
EV Mix, CD146
EV Mix, CD49e
EV Mix, CD8
EV Mix, CD11c
0.25
0.2
0.15
0.1
0.05
0
-0.05
-0.1
-0.15
-0.2
-0.25

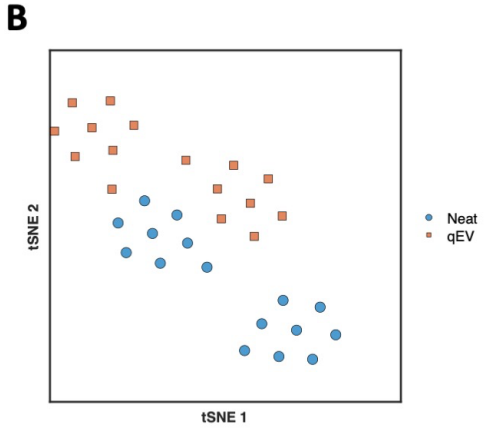
B
tSNE 2
tSNE 1
Neat
qEV

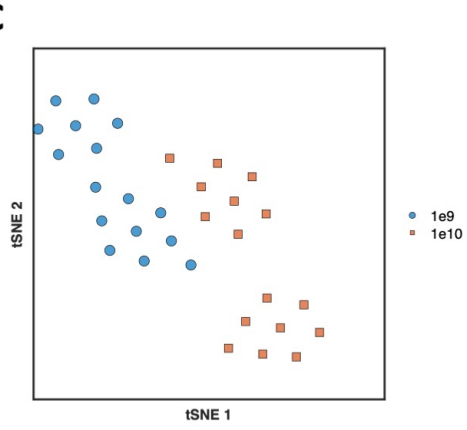
C
tSNE 2
tSNE 1
1e9
1e10

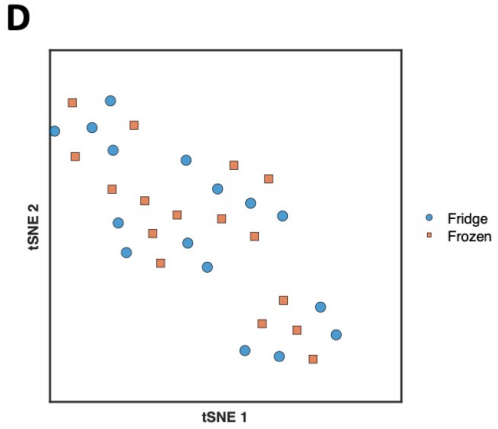
D
tSNE 2
tSNE 1
Fridge
Frozen

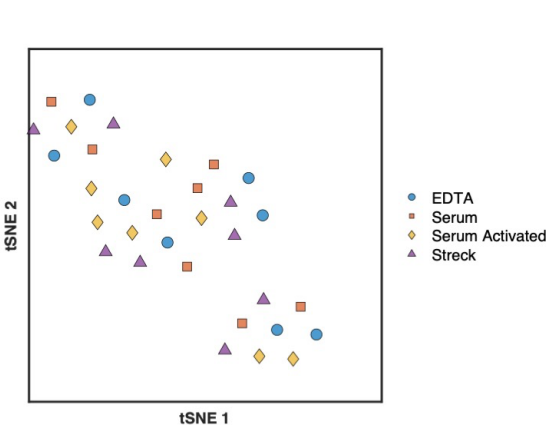
E
tSNE 2
tSNE 1
EDTA
Serum
Serum Activated
Streck

Supplementary Methods 1. Provides a detailed protocol and template for applying the multiplex samples to cell culture EVs that was used to generate data for Figure 1-3.

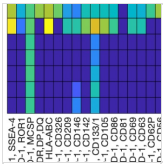

Sep 19, 2020

Multiplexed assay for detection of cell culture EV surface membrane proteins

In 2 collections

Joshua A Welsh[1], Bryce Killingsworth[1], Julia Kepley[1], Tim Traynor[1], Alexis Barfield[1], Jennifer Jones[1]

[1]Translataional Nanobiology Section, Laboratory of Pathology, Center for Cancer Research, National Cancer Institute, National Institutes of Health

dx.doi.org/10.17504/protocols.io.be7yjhpw

Translational Nanobiology Section

Jennifer Jones

DISCLAIMER

This protocol summarizes key steps for a specific type of assay, which is one of a collection of assays used for EV analysis in the NCI Translational Nanobiology Section at the time of submission of this protocol. Appropriate use of this protocol requires careful, cohesive integration with other methods for EV production, isolation, and characterization.

ABSTRACT

Protocol for using Miltenyi Biotec's human MACSplex Exosome Kit to assay one cell-line derived EV sample with up to 3 additional detection antibodies, at two EV count titration points (1E9 and 1E8 per LM10, NanoSight, NTA.). The optimisation of this protocol was done using bead kits released between 2017-2020.

DOI

dx.doi.org/10.17504/protocols.io.be7yjhpw

PROTOCOL CITATION

Joshua A Welsh, Bryce Killingsworth, Julia Kepley, Tim Traynor, Alexis Barfield, Jennifer Jones 2020. Multiplexed assay for detection of cell culture EV surface membrane proteins . **protocols.io** https://dx.doi.org/10.17504/protocols.io.be7yjhpw

COLLECTIONS

Stitched multiplexed assays allow multi-dimensional data analyses of EV repertoires.

2020 Featured Protocols

KEYWORDS

multiplex, flow cytometry, EVs

CREATED

Apr 16, 2020

LAST MODIFIED

Sep 19, 2020

OWNERSHIP HISTORY

Apr 16, 2020 Bryce Killingsworth

Aug 03, 2020 Jennifer Jones

PROTOCOL INTEGER ID

35800

PARENT PROTOCOLS

Part of collection

Stitched multiplexed assays allow multi-dimensional data analyses of EV repertoires.
2020 Featured Protocols

MATERIALS TEXT

MATERIALS

Low Protein Binding Collection Tubes (2.0 mL) **Thermo Fisher Catalog #88379**

MACSPlex Exosome Kit human **Miltenyi Biotec**

AcroPrep Advance Filter Plates for Aqueous Filtration - 350 µL 0.2 µm Supor membrane (10/pkg) **Contributed by users**

DISCLAIMER:

This protocol summarizes key steps for a specific type of assay, which is one of a collection of assays used for EV analysis in the NCI Translational Nanobiology Section at the time of submission of this protocol. Appropriate use of this protocol requires careful, cohesive integration with other methods for EV production, isolation, and characterization.

BEFORE STARTING

- The protocol and attached planning template spreadsheet have been designed for an experiment assaying one cell-line derived EV sample with up to 3 additional detection antibodies, at two EV count titration points (1E9 and 1E8 per LM10, NanoSight, NTA.) Modifications of the spreadsheet and protocol may be necessary to use as a guide to assay multiple samples, human sample-derived EVs, or use additional numbers of detection antibodies.

Experiment planning

1 Determine which antibodies to use to detect EV surface membrane proteins in addition to the included CD9, CD63 and CD81 antibodies. All additional antibodies must be either APC or AF647 conjugated. Ensure you know the concentration of the antibodies, and if you are using an antibody conjugated in-lab, avoid preparations that have unbound dye.

2 Calculate the particle concentration of your EV sample, and the total particle count.

3 Use this template document to input your sample information and generate a plate map to visualize your experiment

Citation: Joshua A Welsh, Bryce Killingsworth, Julia Kepley, Tim Traynor, Alexis Barfield, Jennifer Jones (09/19/2020). Multiplexed assay for detection of cell culture EV surface membrane proteinsÃÂ . https://dx.doi.org/10.17504/protocols.io.be7yjhpw

and the wells you will fill in the 96-well plate to be analyzed by the flow cytometer. Check the "How much volume of your sample is needed for this assay (µL)" section of the sheet to ensure your selections for EV count titration points are reasonable. If you have a very concentrated sample (~5E11part./mL or greater) you should increase the upper EV titration point to increase the fluorescent signal of the assay. If your sample is so dilute that you cannot incubate 1E9 EVs with each detection antibody consider methods to concentrate your sample as the fluorscent signal may be very weak and lower titration points not possible.

2020-07-30 - MACSplex Protocol Template.xltx

Additionally, this template was designed so that the user is directed to transfer a volume of EVs directly from the stock EV preparation into a tube with MACSplex capture beads and MACSplex buffer. However, for the lower titration point(s) the user may wish to prepare dilutions of their EV stocks in PBS and use equal volumes of EV dilutions for all mixes. For example Tube 1 contains 10 µL of a 1E11 part/mL EV dilution and Tube 2 contains 10 µL of a 1E10 part/mL EV dilution.

This template specifically applies to cell culture supernatant derived EVs. It is not recommended to use 10 µL (~15,000 beads) of beads with EVs derived from human fluids, such as plasma or serum as the bead recovery tends to be lower with biofluid ssamples than for cell culture supernatant EV preparations. A higher volume of beads would therefore be required.

4 Below is an example of how you might modify the template spreadsheet plate map to analyze more than one EV sample. Organize the plate so that the multichanel pipette can be used to transfer one antibody solution to a column or row. The "EV - bead capture" section of the spreadsheet will need to be duplicated and modified to help calculate needed volumes for each EV sample.

	1	2	3	4	5	6	7
A	CD9	CD63	CD81	mAb 4	mAb 5	mAb 6	Setup beads
	1E9 EVs	1E9 EVs	1E9 EVs	1E9 EVs	1E9 EVs	1E9 EVs	
	Cell line 1	Cell line 1	Cell line 1	Cell line 1	Cell line 1	Cell line 1	
	10 µL capture beads	10 µL capture beads	10 µL capture beads	10 µL capture beads	10 µL capture beads	10 µL capture beads	
B	CD9	CD63	CD81	mAb 4	mAb 5	mAb 6	5 µL capture beads
	1E8 EVs	1E8 EVs	1E8 EVs	1E8 EVs	1E8 EVs	1E8 EVs	
	Cell line 1	Cell line 1	Cell line 1	Cell line 1	Cell line 1	Cell line 1	
	10 µL capture beads	10 µL capture beads	10 µL capture beads	10 µL capture beads	10 µL capture beads	10 µL capture beads	
C	CD9	CD63	CD81	mAb 4	mAb 5	mAb 6	
	1E9 EVs	1E9 EVs	1E9 EVs	1E9 EVs	1E9 EVs	1E9 EVs	
	Cell line 2	Cell line 2	Cell line 2	Cell line 2	Cell line 2	Cell line 2	
	10 µL capture beads	10 µL capture beads	10 µL capture beads	10 µL capture beads	10 µL capture beads	10 µL capture beads	
D	CD9	CD63	CD81	mAb 4	mAb 5	mAb 6	
	1E8 EVs	1E8 EVs	1E8 EVs	1E8 EVs	1E8 EVs	1E8 EVs	
	Cell line 2	Cell line 2	Cell line 2	Cell line 2	Cell line 2	Cell line 2	
	10 µL capture beads	10 µL capture beads	10 µL capture beads	10 µL capture beads	10 µL capture beads	10 µL capture beads	
E	CD9	CD63	CD81	mAb 4	mAb 5	TGF-B1	
	PBS control	PBS control	PBS control	PBS control	PBS control	PBS control	
	10 µL capture beads	10 µL capture beads	10 µL capture beads	10 µL capture beads	10 µL capture beads	10 µL capture beads	

Citation: Joshua A Welsh, Bryce Killingsworth, Julia Kepley, Tim Traynor, Alexis Barfield, Jennifer Jones (09/19/2020). Multiplexed assay for detection of cell culture EV surface membrane proteinsÃÂ . https://dx.doi.org/10.17504/protocols.io.be7yjhpw

Day 1: Incubating EVs with capture beads

5 Using the "EV - capture bead mix preparation" section of the template as a guide, determine the volumes of MACSplex buffer, MACSplex capture beads, and EVs that will be mixed together for the overnight bead capture incubation.

The spreadsheet has been designed so that the combined volume of MACSplex buffer and EVs in PBS is 65 µL for every 10 µL of MACSplex capture beads, or 75 µL of volume per detection antibody "test.'

6 Prepare an Eppendorf 2.0 mL LoBind collection tube for each EV sample being assayed, but before use ensure that the planned volume to be transferred to the tube is able to invert when the tube is rotated, otherwise the capture beads may sediment at the bottom of the tube during the overnight incubation and prevent proper interaction of EV proteins with their capture antibodies.

Other high quality low-protein binding tubes can be used if necessary.

7 

Using our shared digital inventory, identify which capture bead tube you will use for this experiment and write down the lot number.

> CRITICAL STEP: The lot number is important for potential quality control issues that may arise with any of the 39 different bead populations.

8 Transfer the calculated amount of MACSplex buffer to each EV sample collection tube.

9 Spin down and vortex very thoroughly on the highest setting a tube of human MACSPlex Exosome Capture Beads and aliquot the calculated volumes into each prepared EV sample collection tube.

10 Vortex and then add the calculated volume of undiluted or diluted EVs to each labeled tube containing MACSplex buffer and capture beads.

11 

Vortex each tube well, then place in a tube rotator, covered with foil, and rotate overnight at RT.

> CRITICAL STEP: make sure the volume inside each tube is inverting and falling down the side of the tube when it is rotated so that the large capture beads remain in suspension throughout the night to allow for adequate mixing.

Day 2: Staining captured EVs with detection antibodies

12 Use the "Antibody preparation table" section of the template to calculate the volumes of antibodies and buffer you will need to prepare for the detection antibody staining step of the assay.

Citation: Joshua A Welsh, Bryce Killingsworth, Julia Kepley, Tim Traynor, Alexis Barfield, Jennifer Jones (09/19/2020). Multiplexed assay for detection of cell culture EV surface membrane proteinsÃÂ . https://dx.doi.org/10.17504/protocols.io.be7yjhpw

13 Get 1 new Pall 0.2 µm PES filter plate.

14 Using a multichannel pipet, add 150 µL of MACSplex buffer to all sample and control wells.

It is recommended to use the top portion of the vacuum manifold as a plate holder to aid pipetting.

Screen Shot 2020-07-30 at 10.29.13 PM.png

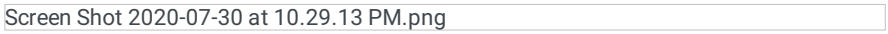

Figure 1: Pall Vacuum Manifold (ID: 5017.) The silver metal top is removable and rests on the blue metal bottom component. The blue pressure valve can be opened slowly to prevent sudden pressure changes disturbing fluid. Vacuum should only be applied until sufficient to empty wells of fluid. The silver metal top can be used as a temporary plate rack for pipetting and mixing samples during washing steps. Figure from Pall's website.

15 Subject the plate to vacuum just until all wells are emptied of buffer.

(release the vacuum pressure gently by pressing the vacuum release rapidly)

Quickly and gently blot the bottom of the filter plate against a clean paper towel.

16 As quickly as possible, add 50 µL of MACSplex buffer to previously wetted wells.

17 Vortex each EV sample tube very thoroughly and add 75 µL to each test well.

75 µL should contain 10 µL of capture beads with EVs bound to them.

Based on the template spreadsheet you should have 10% excess volume so there should be no concern with running out of sample for the last detection well on the filter plate.

(To aspirate all volume at the bottom of the collection tube, the tube may need to be spun down using a bench-top centrifuge and then quickly vortexed or pipetted again.)

18 Add 10 µL of vortexed MACSplex capture beads to the indicated detection antibody control wells (1 per detection antibody.)

19 All detection antibodies should be vortexed gently and spun quickly in a table top centrifuge if possible.

20 Prepare all antibody solutions according to the template spreadsheet. If doing a large experiment make sure to only prepare the antibody solutions immediatley before use.

21 Once antibody solutions are prepared, vacuum the plate until the wells are just empty of liquid. Very quickly and gently blot the bottom of the filter plate against a clean paper towel to remove any drops of buffer on the bottom of the plate.

Citation: Joshua A Welsh, Bryce Killingsworth, Julia Kepley, Tim Traynor, Alexis Barfield, Jennifer Jones (09/19/2020). Multiplexed assay for detection of cell culture EV surface membrane proteinsÃÂ . https://dx.doi.org/10.17504/protocols.io.be7yjhpw

22

Using a multichanel pipette and reagent well if possible, and dispensing quickly to prevent filter plate membranes from drying out, dispense antibody solutions onto their indicated wells, 200 µL of antibody solution per well. Avoid bubble formation and do not mix initially.

CRITICAL STEP: when using the multichanel pipette it is easy to accidentally draw up unequal volumes of solution. Rock the pipette very firmly on the tips to ensure a strong connection, ensure all tips are level by visual inspection before use, when drawing up fluid ensure all tips are fully placed below the top level of the reagent, and **visually confirm** that each tip has a similar amount of fluid. All the fluid should remain at the bottom of the pipette tip and not drift higher up in the tip, otherwise it will not be dispensed equally and bubbles will form in an attempt to eject residual fluid.

23 Using a multichannel pipet set to 100 µL, mix the volumes in the wells up and down, without contacting the filter membranes at the bottom of the wells to avoid puncturing them. The tip should initially be placed exactly in the middle of the fluid in the wells, then rotated slightly toward the sides of the well to mix beads which may be on the side of the well.

Screen Shot 2020-07-30 at 10.48.28 PM.png

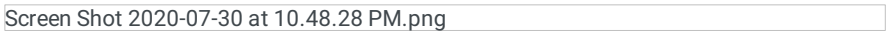

Figure 2: Three ~400 µL wells with a 0.2 µm membrane at the bottom. The triangle represents the optimal placement of the pipette tip during mixing. One scrape of the membrane does not mean the experiment is ruined, but hard scrapes can either puncture a hole in the membrane, allowing bead-captured EVs to spill out, or introduce membrane debris into the sample mixture.

24 Cover the plate with a foil plate sealer and incubate for 2 hours at RT, shaking.

25 After 2 hours, vacuum the plate until fluid just empty, and then add 150 µL of MACSplex buffer to all used wells immediately.

26 Using the 75 µL setting, with the plate positioned on top of the silver metal part of the manifold, reverse pipette all wells with careful tip positioning to avoid bubbles but also not scrape filter membrane.

27 Clear all wells with the vacuum.

28 Immediately added 150 µL buffer to all wells

29 Using the 75 µL setting, with plate positioned on top of manifold, reverse pipette all wells with careful tip positioning to avoid bubbles but also not scrape filter membrane

Citation: Joshua A Welsh, Bryce Killingsworth, Julia Kepley, Tim Traynor, Alexis Barfield, Jennifer Jones (09/19/2020). Multiplexed assay for detection of cell culture EV surface membrane proteinsÃÂ . https://dx.doi.org/10.17504/protocols.io.be7yjhpw

30 Place on vacuum manifold until all wells are cleared

31 Immediately add 200 µL of buffer to all wells.

This final resuspension volume can be adjusted to produce more or less concentrated final suspensions of the capture beads, depending on the optimal concentration to run samples on the flow cytometer.

32 Using 200 µL setting, with plate on top of metal manifold piece, all wells should be reverse pipetted with tip positioning careful to avoid bubbles but also not scrape filter membrane and then transferred to Axygen racked mini 1.1 mL tubes, or a 96-well plate compatable with the plate reader for the particular clow cytometer being used.

When preparing this final resuspension press the mutlichanel plunger half-way to its stopping point to use a volume of ~100 µL to fully resuspend all capture beads sitting on top of the filter plate membrane.

33 Add 5 µL of capture beads in 200 µL of PBS to a free well on the plate or tube rack for the cytometer, as well as 20 µL of setup beads with 20 µL of PBS (varies largely depending on setup bead concentration) to another free well.

Day 2: running plate on cytometer

34 Run setup beads on the flow cytometer to adjust cytometer settings and gate around a single bead population.

35 Analyze the full volume of each 200 µL stained EV sample, including the non-EV containing capture bead + detection antibody controls to check for nonspecific binding of detection antibody to capture beads.

Data analysis

36 Use MPA_{PASS} software to analyze the multiplexed EV protein expression data. Protocol under development.

Citation: Joshua A Welsh, Bryce Killingsworth, Julia Kepley, Tim Traynor, Alexis Barfield, Jennifer Jones (09/19/2020). Multiplexed assay for detection of cell culture EV surface membrane proteinsÃÂ . https://dx.doi.org/10.17504/protocols.io.be7yjhpw

Supplementary Methods 2. Provides a detailed protocol for bead gating strategies using FlowJo Software that was used to generate data for Figure 1-5.

bu3mnyk6

MPAPASS - Gating flow cytometry multiplex data V. (bu3mnyk6)

Joshua A Welsh[1], Sean M Cook[1], Jennifer Jones[1]

[1]Translational Nanobiology Section, Laboratory of Pathology, Center for Cancer Research, National Cancer Institute, National Institutes of Health

1 *Works for me*

Joshua Welsh

DISCLAIMER

This protocol summarizes key steps for a specific type of method, which is one of a collection of methods and assays used for EV analysis in the NCI Translational Nanobiology Section at the time of submission of this protocol. Appropriate use of this protocol requires careful, cohesive integration with other methods for EV production, isolation, and characterization.

ABSTRACT

This is collection contains the protocols required for each step in the mpapass software pipeline for performing stitched multiplex analysis. This is one of a number of protocols in the pipeline for using the mpapass software package and is applicable to the latest release of the software.

PROTOCOL INFO

Joshua A Welsh, Sean M Cook, Jennifer Jones . MPAPASS - Gating flow cytometry multiplex data. **protocols.io**
https://protocols.io/view/mpapass-gating-flow-cytometry-multiplex-data-bu3mnyk6

CREATED

May 17, 2021

LAST MODIFIED

May 17, 2021

PROTOCOL INTEGER ID

49997

MATERIALS TEXT

FlowJo

DISCLAIMER:

This protocol summarizes key steps for a specific type of method, which is one of a collection of methods and assays used for EV analysis in the NCI Translational Nanobiology Section at the time of submission of this protocol. Appropriate use of this protocol requires careful, cohesive integration with other methods for EV production, isolation, and characterization.

Importing the Files into FlowJo

1 Import the desired files into the FlowJo workspace using either the Add Samples (red box) button under the FlowJo tab (blue box), or simply drag the desired files into FlowJo.

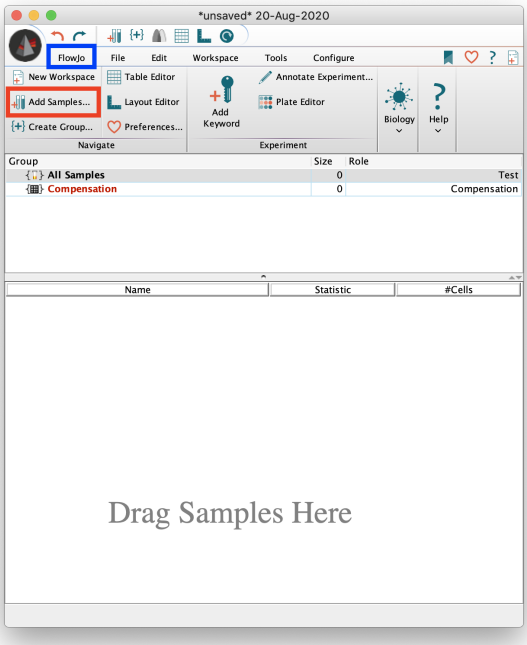

It is recommended that the fluorescence parameters be calibrated into standard units of 'molecules of equivalent soluble fluorophore' (MESF) to aid in reproducibility of data. This can be done using FCMPASS software in combination with commercially available MESF beads. See the FCMPASS software for further information at https://nano.ccr.cancer.gov/fcmpass

Gating the Bead Populations

2 Double-click on any of the samples in order to bring up a scatter plot. Change the parameters of the scatter plot to FSC-A and SSC-A channels and gate around the single events using a rectangular gate.

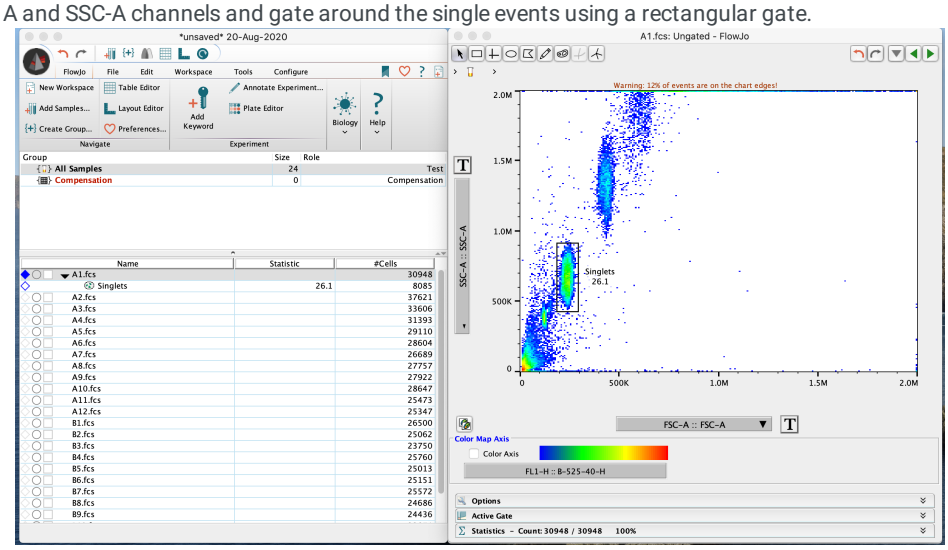

In this example, the A1.fcs sample was used to gate for singlets.

3 Double-click on the newly gated Singlets population to open a new scatter plot. Change the parameters to the FITC-A and PE-A channels, and a pattern similar to the figure below should be seen.

There are supposed to be 39 distinct bead populations, however in kits manufactured between 2018-2019, only 38 can be seen due to the merging of the 89 and 99 bead populations.

image.png

4 Each of the distinct populations corresponds to a antibody coated bead that can be determined from the bead legend below:

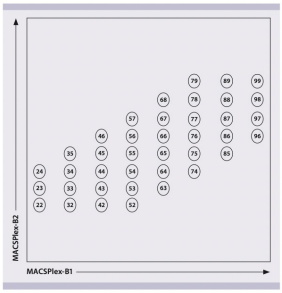

No.	Antibody	Isotype
22	CD3	mIgG2a
23	CD4	mIgG2a
24	CD19	mIgG1
32	CD8	mIgG2a
33	HLA-DRDPDQ	REA
34	CD56	REA
35	CD105	mIgG1
42	CD2	mIgG2b
43	CD1c	mIgG2a
44	CD25	mIgG1
45	CD49e	mIgG2b
46	ROR1	mIgG1κ
52	CD209	mIgG1
53	CD9	mIgG1
54	SSEA-4	REA
55	HLA-ABC	REA
56	CD63	mIgG1κ
57	CD40	mIgG1κ
63	CD62P	REA
64	CD11c	mIgG2b

No	Antibody	Isotype
65	CD81	REA
66	MCSP	mIgG1
67	CD146	mIgG1
68	CD41b	REA
74	CD42a	REA
75	CD24	mIgG1
76	CD86	mIgG1
77	CD44	mIgG1
78	CD326	mIgG1
79	CD133/1	mIgG1κ
85	CD29	mIgG1κ
86	CD69	mIgG1κ
87	CD142	mIgG1κ
88	CD45	mIgG2a
89	CD31	mIgG1
96	REA Control	REA
97	CD20	mIgG1
98	CD14	mIgG2a
99	mIgG1 control	mIgG1

Table 1.1: Overview of surface marker antibodies used for the MACSPlex Exosome Kit.

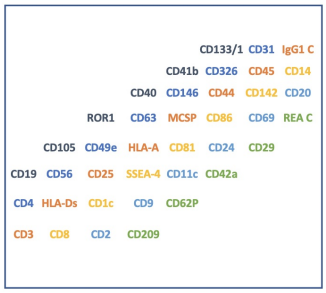

5 Gate each of the bead populations using a elliptical gate and label the populations according to the bead legend in step 4. For the merged population, gate around the entire population--later the population wil be separated.

image.png

Separating the Merged Population

6 On select cytometers it has been found that some lots of Miltenyi exosome multilpex beads do not adequately separate populations 89 and 99. If this is not the case proceed to the next section.

The FlowJo workspace should now have subpopulations under the Singlet population for each bead population as well as the merged population.

Click on the sample used to gate the bead populations (the highlighted A1.fcs sample in the figure below) and then navigate to the tools tab (blue box).

Click on Derive Parameters (red box) which will bring up a new window.

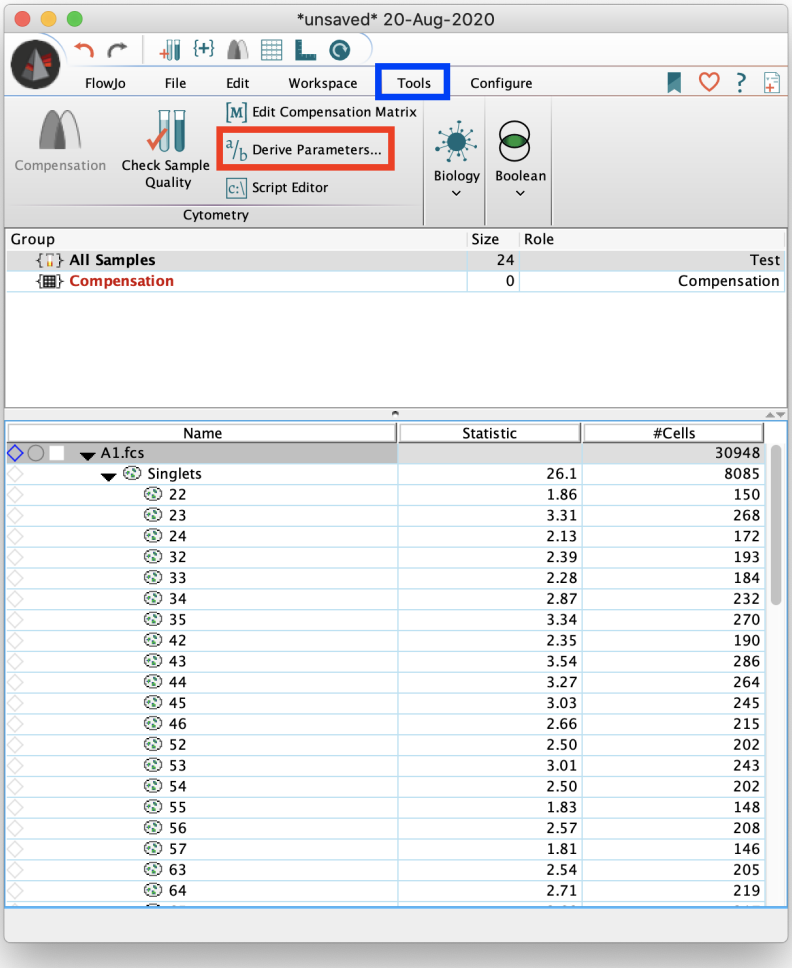

7 Creating the Derived Parameter:

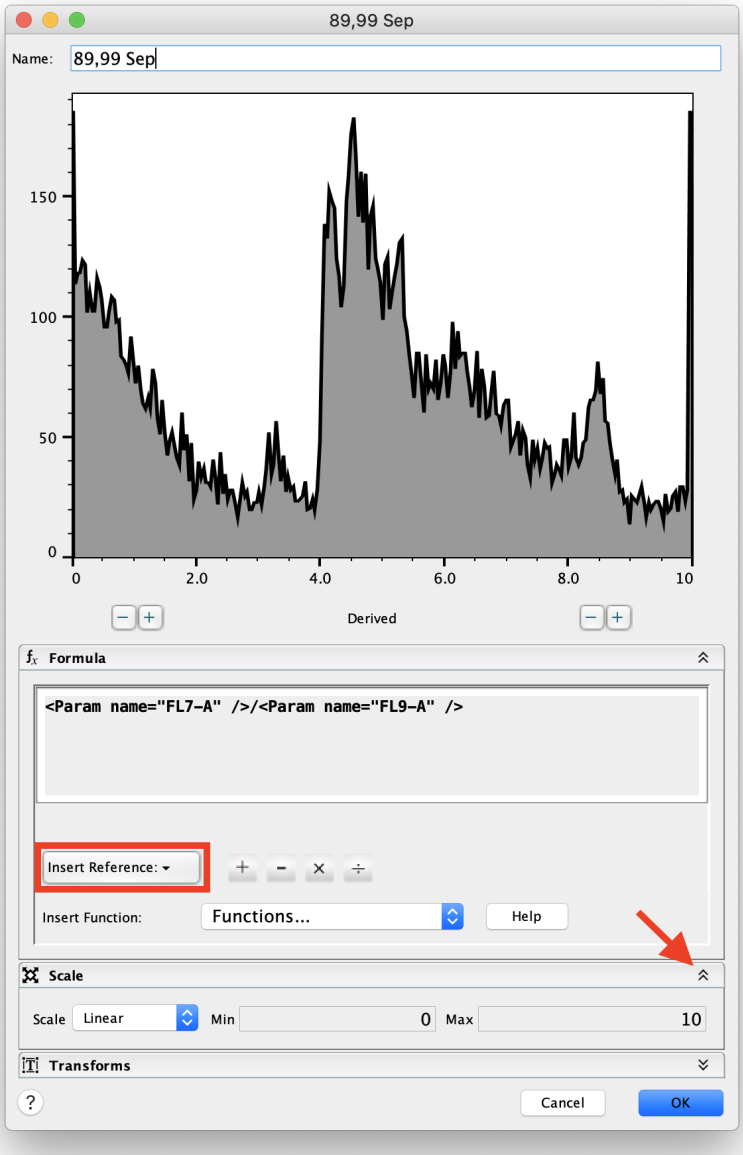

7.1 In this new window, at the top, name the derived parameter 89,99 Sep.

7.2 Using the Insert Reference button (red box), choose the V-525-A channel. A string of characters will appear in the text box above.

Click on the division button next to the Insert Reference button.

Once again using the Insert Reference button (red box), now choose the V-660-A channel.

A plot similar to the figure above should be now be seen

7.3 Click on the collapse/open arrows for the Scale tab (denoted by a red arrow).

Choose the Linear scale and set the Min to 0 and the Max to 10.

Now click OK, and the derived parameter should appear beneath the chosen sample.

8 Gating the Merged Population:

8.1 Click on the 89_99 subpopulation to open a new scatter plot.

Choose 89,99 Sep derived parameter from the dropdown menu on the X-axis and the histogram option on the Y-axis.

A plot similar to the figure below should be seen.

8.2 Click on the Bisector Tool (red arrow) to gate the two bead populations. Make sure to choose a point where the two populations are distinctly separated.

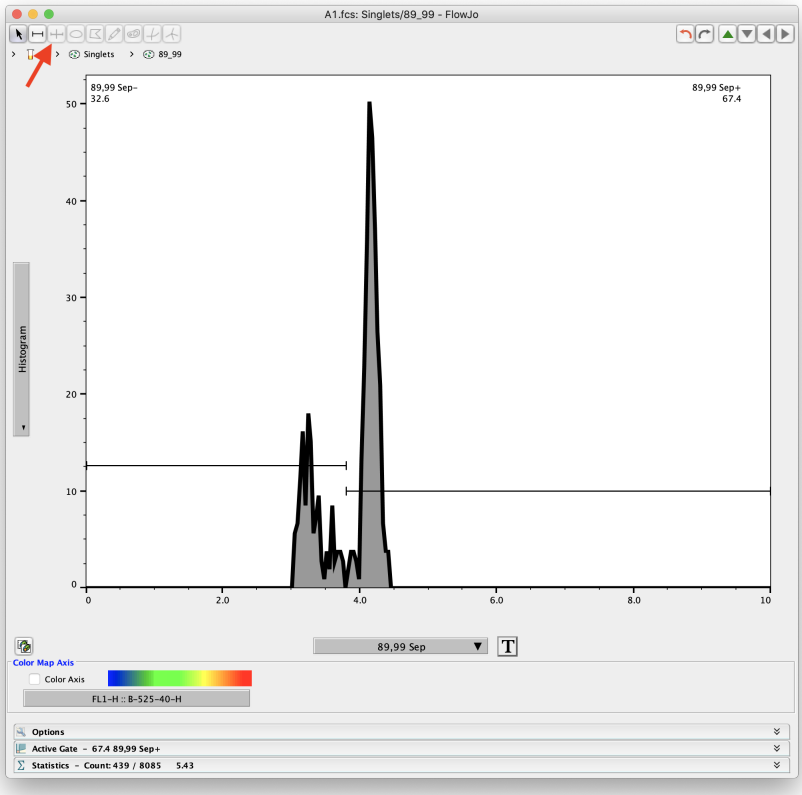

8.3 The populations should be relabeled by right clicking the populations in the FlowJo workspace. The upper population should be labeled 99 while the lower population should be labeled 89.

Applying the Gates to Each Sample

9 In the FlowJo workspace, highlight all the gated populations and the derived parameter.

Now drag them into All Samples Group above (red arrow).

All files in the FlowJo workspace should now be gated exactly how we gated our chosen sample. This will be reflected in the FlowJo workspace as all samples should now have the same populations.

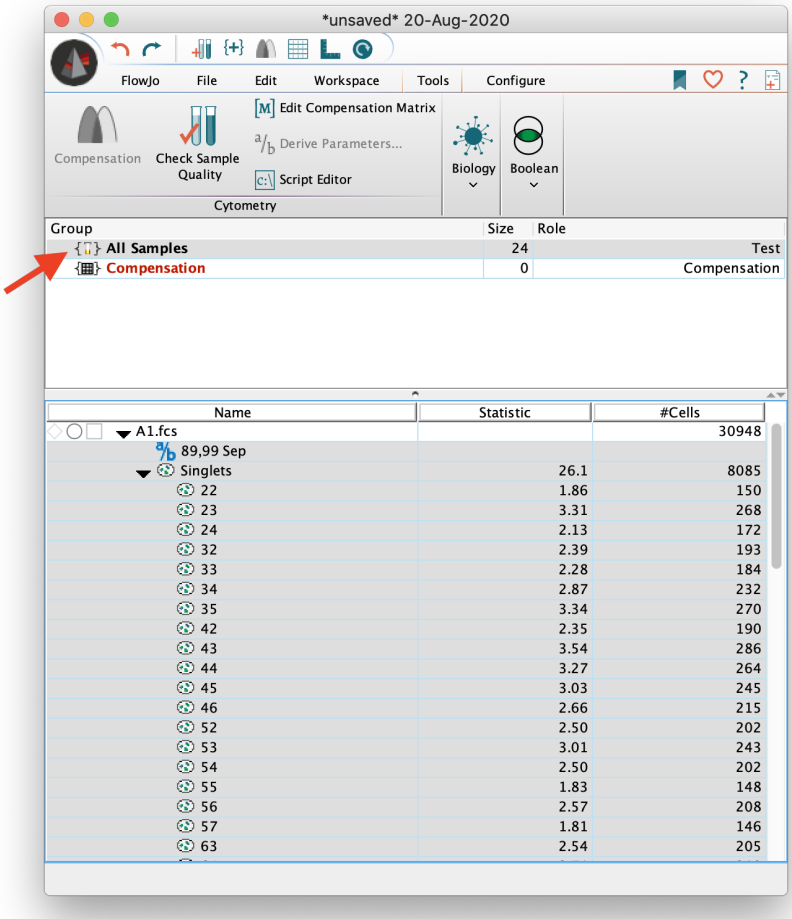

Exporting the Files

10 Now that all our samples have been gated, it is time to export the data from FlowJo into .csv files.

For any of the samples select all the bead populations to export, then under the Edit tab (blue box), click the Select Equivalent Nodes button to select all bead populations from every sample to export.

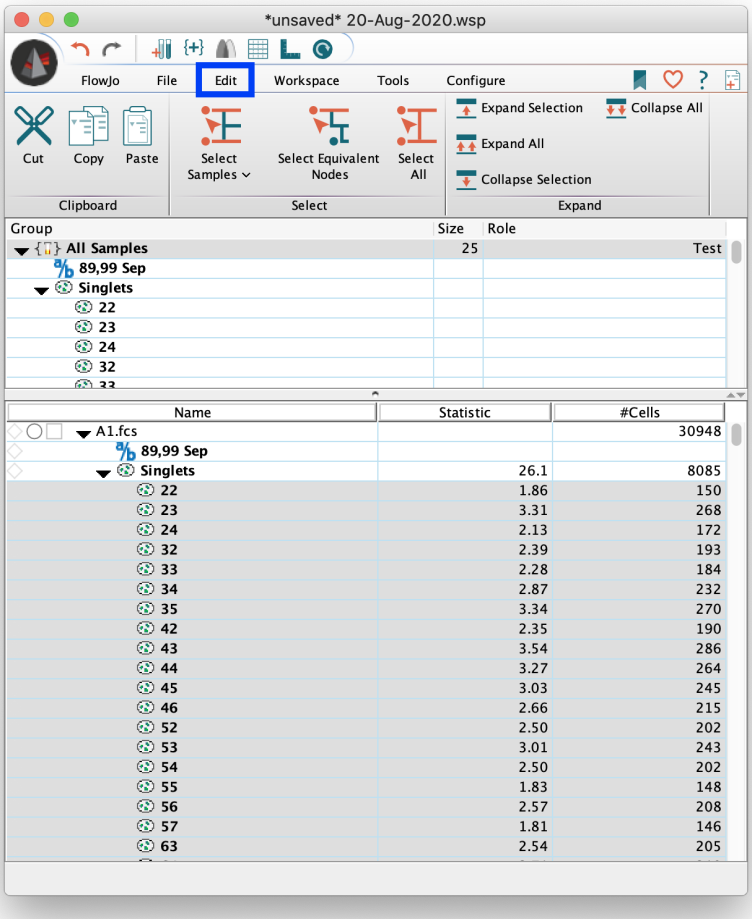

11 Navigate to the file tab and click on the Export/Concatenate Populations button.

12 Change the format to CSV - Scale Values.

Uncheck 'Include Header'

Change the Destination to desired folder.

Click on Custom Set of Parameters and then the View/Edit button directly next to it. Choose the APC parameter from the pop-up list.

Finally click Export to generate the .csv files in the destination folder.

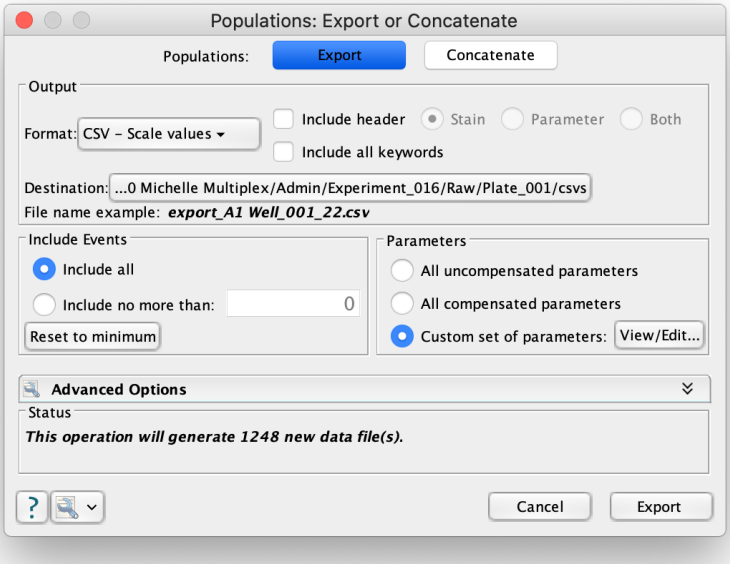

13 In preparation for the MPAPASS software, you will have to manually rename the 99 bead population from the export suffix of 89_99_99.csv to simply _99.csv

Repeat if this occurs with the 89 bead population.